G109.1-1.0: A Supernova Remnant Interacting with a Molecular Cloud

(分子雲と相互作用する超新星残骸 G109.1-1.0)

Ken'ichi Tatematsu
(立松健一)

G109.1-1.0: A Supernova Remnant Interacting with a Molecular Cloud

Ken'ichi Tatematsu

Submitted in partial fulfillment of
the requirements for the degree of
Doctor of Science
in Faculty of Science
Nagoya University

ABSTRACT

The molecular cloud in the vicinity of the peculiar supernova remnant G109.1-1.0 has been observed in the J = 1-0 transitions of CO molecules. The Nagoya 4 m radio telescope and the Nobeyama 45 m radio telescope were used for the observations. It is found that the main molecular cloud on the west has prevented an isotropic expansion of G109.1-1.0 causing its semicircular shape of this remnant. The CO arm extending from the main molecular cloud shows an apparent anticorrelation with the curled X-ray feature seen in G109.1-1.0 called the X-ray jetlike feature. The CO arm is found to consist of two thin CO filaments. At least one of these filaments should be located near the rear remnant shell. Molecules which were located in a thin (< 0.5 pc) original surface layer of the molecular cloud are thought to have been fully dissociated due to the SNR shock. It is expected that the momentum deposited in the cloud shock will compress the molecular cloud to some extent in 10^5-10^6 yr. The X-ray jetlike feature probably represents the density distribution of the hot plasma in this SNR. Three explanations for this feature are proposed, and there is a possibility that the existence of the molecular cloud has contributed to the formation of this feature. The present observations have clearly revealed that G109.1-1.0 accompanies the molecular cloud and that they interact with each other.

Subject headings: interstellar: molecules

- nebulae: individual (G109.1-1.0)

- nebulae: supernova remnants - X-rays: sources

ACKNOWLEDGMENTS

I would like to express my hearty thanks to Yasuo Fukui for fruitful discussions. I have benefited from his insight into astrophysics. I thank Kin-aki Kawabata for pertinent advice and many helpful comments. Thanks are also due to Hideo Ogawa for his critical comments and his excellent work on development of the receiver system of the 4 m radio telescope. I wish to acknowledge valuable discussions with Makoto Nakano, Tomokazu Kogure, Tomoyuki Hanawa, Kohji Tomisaka, and Satoshi Yamamoto. I thank Takahiro Iwata for assistance during the observations at Nobeyama. Frederick D. Seward kindly provided me with the energy divided X-ray data of G109.1-1.0, which are greatly helpful for discussion in this thesis. This work was in part financially supported by the Grant-in-Aids for Scientific Research of the Ministry of Education, Science, and Culture of Japan (Nos. 59420002, 60302014, and 60790097).

Table of Contents

I. INTRODUCTION

A. Supernova Remnants (SNRs) and Their Evolution

The supernova (SN) is an explosion phenomenon at the final stage of the evolution of massive ($> 8\ M_{\odot}$) stars or accreting stars in the binary systems. After the supernova explosion, the ejecta from the progenitor (precursor star) begin to expand at supersonic velocity. The expanding shock having the hot gas interior is formed, and it is called a supernova remnant (SNR). It gathers the ambient interstellar medium through the expanding shock and heats it up. The interior of the SNR is a hot gas. The total energy of the SNR is $\sim 10^{51}$ ergs. The number of the known SNRs in our Galaxy (the Milky Way Galaxy) is around 150. The SNR is classified into three categories: the shell type, the plerionic type, and the composite type (e. g., Weiler 1985). The shell type is the most popular ($\sim$ 80 %). This type is characterized by the shell structure in the radio-continuum image and the steep radio spectral index $\alpha < -0.3$, where $I_{\nu} = \text{const}\ \nu^{\alpha}$. The plerionic type has a filled-center form (intensity maximum is located at the center) in the radio continuum emission and shows the flat radio spectral index $\alpha > -0.3$. The activity of this type SNR is believed to be supported by the central stellar remnant or pulsar. The composite type has both of a shell activity and a stellar remnant activity. The evolution of the shell-type SNR is described here, because the properties of the

plerionic and composite types have not been well known yet. We assume the typical intercloud medium with an atomic number density of order 0.1 cm^{-3} as the ambient matter of the SNR.

At the beginning of the expansion, the ejecta from the progenitor are a main component of the SNR. The SNR expands freely, and has a constant expansion velocity of $\sim 10^4$ km s^{-1}. After the mass of the interstellar medium swept by the SNR shell becomes larger than that of the ejecta (age t $\sim$ 60 yr), the SNR enters the adiabatic or Sedov (1959) phase. At this stage the temperature of the interior hot plasma of the SNR is so high ($> 10^6$ K) that radiation loss is negligible. Therefore the total energy of the SNR is assumed to be constant or equal to the initial energy of the SNR. The temperature of the SNR decreases with the age, and reaches 1×10^6 K at an age of t $\sim 10^4$ yr. When the temperature becomes below 10^6 K, radiative cooling of the hot gas becomes effective. At this stage the energy does not conserve, and the SNR shell expands conserving its momentum. This stage is called the snowplow phase.

The Cygnus Loop and the Crab Nebula are famous examples of the SNRs. The Crab Nebula is a young (t $\sim$ 900 yr) plerionic-type SNR, and the Cygnus Loop is a shell-type SNR at the latest stage of the Sedov phase.

B. Importance of the Interaction of the SNRs with the Interstellar Medium

The supernova (remnant), which is one of the most energetic astronomical objects, must have a significant influence on the interstellar medium. It will change the structure, density, temperature, phase, velocity field, and magnetic field of the interstellar medium. The interstellar medium consists of gases having various physical conditions. The temperature ranges $10\text{-}10^6$ K, and the number density of hydrogen atoms ranges $10^{-1}\text{-}10^4$ cm^{-3} or denser. Molecular cloud is the densest part of the interstellar medium, and mainly consists of a molecular gas. The structure of the ambient matter will determine the evolution of the SNR and the energy transfer into the interstellar medium. In particular, the encounter of the SNR shell with the molecular cloud causes the appreciable decrease of the SNR energy mainly through the radiative cooling, whereas the enormous energy and momentum will be injected into the molecular cloud. The compression of the the interstellar medium is thought to initialize the birth of stars (Öpik 1953). The molecular cloud is the site where stars are born, and hence the compression of the molecular cloud by the SNR must be important as a potential trigger for the star formation. The rather old SNRs breaking through the galactic disk will produce the outflow of the hot gas from the galactic disk, and this hot gas will maintain the galactic hot gaseous halo (e. g., Tomisaka and Ikeuchi; also see

Heiles 1987). Therefore the history of the SNR evolution will determine the properties of the galactic halo.

C. Previous Studies on the Interaction of SNRs with Molecular Clouds

Studies of interaction between SNRs and molecular clouds began with Wootten's (1977) CO observations toward W44. Following his observations, several groups have searched indications of the interaction: e. g., Wootten's (1981) observations toward W28, Dame's (1983) observations toward W44, and the observations of W50 by Huang, Dame, and Thaddeus (1983). However, some of the results of the previous searches, in particular toward the inner Galaxy (where the galactocentric distance is less than 10 kpc; we assume throughout this thesis the distance to the galactic center from the sun is 10 kpc), are difficult to interpret because of confusion due to unrelated molecular clouds along the line of sight. According to our reexamination of the published data, it seems that there are only two convincing examples of the interaction. One is the broad molecular-line emission discovered in IC 443 (DeNoyer 1979; DeNoyer and Frerking 1981; White et al. 1987). The linewidth of the molecular emission is up to $\sim$100 km s^{-1}, and is thought to be a postshock molecular gas shocked by the SNR. The broad CO emission obtained by Huang, Dickman, and Snell (1986) with the 14 m radio telescope at the Five College Radio Astronomy Observatory (FCRAO) is distributed at several distinct small regions with a typical size of 3'. In spite

of searches for another example, IC 443 has been the unique convincing example until now. The other example of the interaction is the compression of the western rim of the Cygnus Loop by the two small molecular clouds with a size of a few pc (Scoville et al. 1977). The radio and optical intensities of the SNR are enhanced at the compressed part of the shell adjacent to the molecular clouds. The number of the convincing examples of the interaction is too small to understand this phenomenon well. It is essential to increase the number of convincing examples to realize the interaction. To obtain new examples of the interaction, we have observed three SNRs. I report here the observations of G109.1-1.0, which were observed with the Nagoya 4 m and the Nobeyama 45 m radio telescopes. The observations with the 4 m radio telescope toward G78.2+2.1 and HB 21 are summarized in Fukui and Tatematsu (1987).

D. Introduction to G109.1-1.0

The SNR G109.1-1.0 (CTB 109) was discovered by Gregory and Fahlman (1980) with an X-ray astronomical satellite, the Einstein Observatory. It has an unusual semicircular shell with a diameter of 30' (Fig. 1). The X-ray pulsar 1E2259+586 is located at the center of the curvature of the shell (Fahlman and Gregory 1981). The pulse period obtained by Fahlman and Gregory (1981) for the first time was 3.5 s, and later this value was revised to 7 s (Fahlman and Gregory 1983). The spin-down rate of the X-ray pulse period is

5×10^{-13} s s^{-1} (Koyama, Hoshi, and Nagase 1987). The optical counterpart of the X-ray pulsar is a faint ($m_B \sim 23.5$ mag) star, and this X-ray pulsar is thought to represent a low-mass binary system (Fahlman and Gregory 1983). The infrared pulsations observed toward it with a pulse period of 3.5 s are probably the second harmonic pulsations (Middleditch, Pennypacker, and Burns 1983). The orbital period of the binary system is $\sim$ 2300 s (Fahlman and Gregory 1983). The curled X-ray ridge (X-ray jetlike feature) extends from the X-ray pulsar toward the northeastern part of the shell (Gregory and Fahlman 1980). At radio wavelengths, this remnant has the semicircular shell, whereas there is no radio feature corresponding to the X-ray pulsar nor the X-ray jetlike feature (Downes 1983; Sofue, Takahara, and Hirabayashi 1983; Gregory et al. 1983; Hughes et al. 1984). The SNR contains one curled radio arc inside the shell. The 10 GHz map obtained by Sofue, Takahara, and Hirabayashi (1983) with the Nobeyama 45 m radio telescope is reproduced in Fig. 2. The spectral index of this SNR ranges from -0.6 to -0.5 (Sofue, Takahara, and Hirabayashi 1983; Hughes et al. 1984). Tatematsu et al. (1987) detected the linear polarization of the radio continuum emission using the Nobeyama 45 m radio telescope, and the degree of polarization at 10 GHz ranges several to 30%. There are several faint optical filaments around the two radio peaks (Hughes, Harten, and van den Bergh 1981), and the optical spectrum of one of the filaments was obtained by Blair and Kirshner (1981). Gregory and Fahlman (1981, 1983) proposed a precessing jet model analogous to SS 433 (e.g., Seward

et al. 1980; Grindlay et al. 1984) on the basis of the presence of the X-ray pulsar, the X-ray jetlike feature, and the radio arc in G109.1-1.0. According to them the X-ray jetlike feature represents the hot gas of the precessing jet. The age of the SNR is $\sim 1.5 \times 10^4$ yr (Sofue, Takahara, and Hirabayashi 1983), and this SNR is thought to be at the latest stage of the Sedov phase.

There is a giant molecular cloud S147/S153 on the west of the remnant (Israel 1980; Heydari-Malayeri, Kahane, and Lucas 1981; Tatematsu et al. 1985). This giant molecular cloud contains five Sharpless (1959) HII regions, gaseous nebulae ionized by massive stars: S147, S148, S149, S152, and S153. The radio pulsar PSR 2255+58 [R. A. = $22^h55^m54^s.2$, Decl. = $58^o53'10''$] with a distance of 4.3 kpc (Davis, Lyne, and Seiradakis 1972; Manchester and Taylor 1981) is located near the molecular cloud. They illustrate massive-star formation activities of this molecular cloud. Fig. 3 shows the overall structure of the giant molecular cloud S147/S153 obtained by using the Nagoya 4 m radio telescope with the room-temperature Schottky receiver (Tatematsu et al. 1985). The abscissa is right ascension (R. A.) and the ordinate is declination (Decl.) for the epoch 1950.0, which are equatorial coordinates on the celestial sphere. The HII region S152 corresponds to a local maximum in the CO intensity. The CO peak at S152 has a radial velocity V_{LSR} with respect to the stars in the solar neighborhood (the local standard of rest, LSR) of $\sim$ -50 km s^{-1}. This molecular cloud has an extent of $\sim 70' \times 25'$ or $\sim$ 80 pc $\times$

30 pc (1 pc = 3×10^{18} cm). The mass is deduced to be 6.1×10^{4} $M_{\odot}$. Tatematsu et al. (1985) discussed the possibility of the interaction on the basis of the CO observations with the old receiver of the 4 m telescope. However it was a problem that there is an apparent gap between G109.1-1.0 and the molecular cloud in Fig. 3. It seems necessary to investigate whether the apparent gap is due to the limited sensitivity or not.

The purpose of the present study is to investigate the relationship between G109.1-1.0 and the giant molecular cloud S147/S153 by observing the 2.6 mm line of CO molecules with sufficient sensitivity and angular resolution. The adopted distance to G109.1-1.0 is 4.1 kpc (Sofue, Takahara, and Hirabayashi 1983).

II. OBSERVATIONS

A. The Nagoya 4 m Radio Telescope

Observations with the Nagoya 4 m radio telescope were made in 1985 January-May. Details of this telescope are described by Kawabata et al. (1985). The J = 1-0 transitions of CO (115.271 GHz) and ^{13}CO (110.201 GHz) were observed. This telescope is a Cassegrain type and is mounted on an alt-azimuth mounting. The primary parabolic reflector of the telescope has a diameter of 4 m and an f/D (focal length by diameter) ratio of 0.493. The surface accuracy of the main reflector is better than 40 μm rms. The half-power beamwidth (HPBW) is 2'.7 at 110 GHz. The main beam efficiency η_M is 0.74±0.05, and the forward spillover and scattering efficiency η_{fss} (Kutner and Ulich 1981) is 0.81±0.06. The receiver front-end used for the present observations was a 15 K cooled GaAs Schottky diode mixer followed by a 1.50±0.25 GHz GaAs FET IF amplifier. The receiver had a receiver temperature of 200-250 K (DSB). This value is 1/4 of the receiver temperature 700-1000 K (DSB) of the old receiver used in the our previous observations (Tatematsu et al. 1985). The back-end was an acousto-optical spectrometer (AOS) with 40 kHz resolution and 44 MHz bandwidth (Takano et al. 1983). The computer system for the telescope control was a NOVA 4/X. Pointing of the telescope was established by observing a number of bright stars with a small optical telescope attached to the radio telescope and

by observing the edge of the solar disk at 110-115 GHz. The accuracy of pointing was known to be better than 20". The employed spacing interval was 3' or 1'.5. Most of the observations were made in the frequency switching mode, whereas some of the spectra were obtained in the position switching mode. The observed spectra contain artificial baselines, and they must be subtracted in data reduction. Third order polynomials were subtracted from the frequency-switched spectra, and linear baselines were subtracted from the position-switched spectra. All spectra were convolved to a resolution of 0.3 km s^{-1} for improving the S/N ratio. The typical rms noise levels for CO and ^{13}CO at this resolution are 0.7 K and 0.1 K, respectively. The intensity was calibrated by using the standard chopper-wheel method (Penzias and Burrus 1973; Davis and Vanden Bout 1973). The intensity is finally expressed in terms of the corrected antenna temperature T_A^* (see Kutner and Ulich 1981). The slight change in the sideband ratio had an influence on the temperature scale. We calibrated the intensity referring to the standard source, Ori A (65.0 K in CO and 11.0 K in ^{13}CO).

B. The Nobeyama 45 m Radio Telescope

Observations were carried out in the J = 1-0 transition of CO in two periods, 1986 December and 1987 April. The 45 m telescope has a half-power beamwidth of 17"$\pm$1" and a main beam efficiency of 0.45$\pm$0.05 at this frequency. The cooled Schottky diode receiver covering 85-115 GHz was used for the

observations, and it provided a system temperature of 800-1000 K (SSB). One of the acousto-optical spectrometers with a resolution of 37 kHz (0.1 km s^{-1}) was employed. For establishing the pointing of the telescope, an SiO maser source was observed in SiO (v = 1, J = 1-0) at 43 GHz every two hours in the observations at least. The pointing accuracy was typically 5"-10". The CO observations were made at spacings of 30"-60". All spectra were obtained in the position switching mode, and linear baselines were subtracted from them. The typical rms noise level is 0.8 K at 37 kHz (0.1 km s^{-1}) resolution. The intensity was calibrated by using the standard chopper-wheel method. The intensity obtained with the 45 m radio telescope was systematically lower than the correct value, because the adjustment of the image-rejection filter used for the 85-115 GHz receiver was incomplete between 1985 January and 1987 May. The intensity was multiplied by 1.50, which was determined by observing a few standard CO sources. The intensity is expressed in terms of the corrected antenna temperature T_A^*.

III. RESULTS

A. CO Distribution Obtained with the 4 m Radio Telescope

In this subsection the results obtained with the 4 m radio telescope are described. Figs. 4-6 show the contour map of the CO (J = 1-0) intensity integrated over the radial velocity range V_{LSR} = (-55, -45) km s^{-1} as thick lines. Observed points are illustrated in Fig. 4. This integrated CO map is superimposed upon the X-ray map of G109.1-1.0 (Gregory et al. 1983) in Fig. 5, and is superimposed upon the map of 10 GHz radio continuum emission (Sofue, Takahara, and Hirabayashi 1983) in Fig. 6. The CO intensity maximum on the western edge of the map corresponds to the HII region S152 [R. A. (1950) = $22^h56^m.7$, Decl. (1950) = $58^o32'$]. The main molecular cloud centered at S152 has a weakly concave boundary at R. A. (1950) = 22^h58^m. It is remarkable that G109.1-1.0 has a western boundary, a chord of the semicircular shape, just along this boundary of the main molecular cloud. There is a ridge extending from the main molecular cloud to the east along Decl. (1950) = $58^o45'$. We call it the CO arm. Fig. 7 illustrates CO and ^{13}CO profiles toward the CO intensity maximum at the top of the CO arm [R. A. (1950) = $22^h59^m50^s$, Decl. (1950) = $58^o45'00''$]. In Fig. 5 the CO arm shows an apparent anticorrelation with the X-ray jetlike feature (hatched); the CO arm seems to be surrounded by the X-ray jetlike feature. The X-ray intensity in the area of the CO arm is about 0.6 times that in the X-ray jetlike feature. The radio continuum emission is also weak

at the CO arm area. There is a small molecular cloud on the eastern side of G109.1-1.0 [R. A. = $23^h01^m.7$, Decl. = $58^o42'$], which was discovered in the present observations. This small molecular cloud shows a radial-velocity gradient of +0.2 km s^{-1} pc^{-1} from the east to the west.

B. CO Distribution Obtained with the 45 m Radio Telescope

The area observed with the Nobeyama 45 m radio telescope and the employed spacing interval are illustrated in Fig. 8. The obtained CO maps with 30"-60" resolution are shown in Figs. 9-12. Fig 9 shows the distribution of the CO (J = 1-0) intensity integrated over the radial-velocity range V_{LSR} = (-57, -43) km s^{-1}. The CO emission from the main molecular cloud and the CO arm predominantly lies within the velocity range V_{LSR} = (-53, -47) km s^{-1}. There is no evidence of the broad line emission representing the shocked molecular gas in contrast with the case of IC 443. Fig. 10 shows the CO map integrated over V_{LSR} = (-53, -47) km s^{-1} superimposed upon the 0.1-4.5 keV X-ray map taken from Gregory et al. (1983). These maps give details of the distribution of the molecular cloud, although the distribution is basically the same as that obtained with the 4 m radio telescope. The interface between the main molecular cloud and G109.1-1.0 is clearly seen in Fig. 10. The main molecular cloud, which extends toward the boundary of G109.1-1.0, is observed with the range V_{LSR} = (-53, -49) km s^{-1}. It seems to be very clumpy or spongy: it probably consists of many filamentary

or sheetlike molecular clouds. There is no significant enhancement in the CO intensity along the interface between the main molecular cloud and G109.1-1.0.

The present observations with the 45 m radio telescope show that the CO arm, which is observed as one ridge in the 4 m telescope map, consists of two remarkably thin filaments having different velocities. The map of the CO arm for V_{LSR} = (-51, -49) km s^{-1} is superimposed upon the X-ray map in Fig. 11, and that for V_{LSR} = (-49, -47) km s^{-1} in Fig. 12. One of the two CO filaments seen in Fig. 11 is a curled one, and the other seen in Fig. 12 is a fairly straight one. The western half of the straight filament is observed over V_{LSR} = (-49, -45) km s^{-1}. These two CO filaments emanate from a common root [R. A. (1950) = $22^h58^m20^s$-40^s, Decl. (1950) = $58^o43'$] and reach a common top which is a CO peak [R. A. (1950) = $22^h59^m50^s$, Decl. (1950) = $58^o45'$]. They have a width of $\sim$ 2' (2 pc) and a length of $\sim$15' (18 pc). It is remarkable that these CO filaments appear to delineate the inner boundary of the X-ray jetlike feature (Figs. 11 and 12). In Fig. 9, there are several small molecular clouds in the area of G109.1-1.0. Some of them seem to be located just outside the X-ray jetlike feature. Fig. 13 shows a position-velocity diagram along Decl. (1950) = $58^o45'30''$ parallel to the CO filaments. There is an abrupt change in the radial velocity at R. A. (1950) = $22^h58^m51^s$ in this diagram.

C. Column Density and Mass of the CO Arm

The area of the CO arm has been observed in both of CO

and ^{13}CO lines with the 4 m radio telescope. The distribution of the column density of H_2 molecules in the CO arm is obtained as described in Appendix A. Fig. 14 shows that the northern half of the CO arm has larger column density than the southern half. The straight CO filament probably has larger column density than the curled filament. Toward the CO intensity maximum [R. A. = $22^h59^m.8$, Decl. = $58^o45'$] the H_2 column density is estimated to be 2×10^{21} cm^{-2}. If the CO emission fills the telescope beam uniformly at this position, the mass within the telescope beam area is deduced to be 5×10^2 $M_\odot$. The typical value of the H_2 column density at the diffuse part of the CO arm [R. A. = $22^h58^m.3$-$59^m.4$, Decl. = $58^o45'$] ranges 8-10 $\times$ 10^{20} cm^{-2}. This value is thought to represent the H_2 column density of the straight filament. Toward the curled filament the ^{13}CO intensity is weak ($\sim$ 0.3 K). Therefore the estimation of the column density for the curled filament is not so easy. The observed point at R. A. = $22^h59^m.1$, Decl. = $58^o42'$ is chosen as a representative for the curled filament, and the H_2 column density is roughly deduced to be 1-2 $\times$ 10^{20} cm^{-2}. For evaluating the masses of the two filaments, the masses in the ranges V_{LSR} = (-51, -49) km s^{-1} and V_{LSR} = (-49, -45) km s^{-1} are attributed to the curled and straight filaments, respectively. The curled one has a mass of 4 $\times$ 10^2 $M_\odot$, and the straight one has a mass of 1.6 $\times$ 10^3 $M_\odot$.

The mass of the hot plasma in G109.1-1.0 is estimated to be $\sim$ 1.3×10^2 $M_\odot$ by assuming a typical preshock density of 0.3 m_H cm^{-3}. Either of the two CO filaments has a larger

mass than the plasma of the SNR.

IV. ENERGY DIVIDED X-RAY DATA

A set of X-ray maps corresponding to different energy bands is very helpful in investigating the degree of the X-ray absorption by the molecular cloud. The IPC (Imaging Proportional Counter) detector on the Einstein Observatory (Giacconi et al. 1979), which was used for the observations of G109.1-1.0, was sensitive to X-rays with an energy of 0.1-4.5 keV. Both of the gray-scale map shown in Gregory and Fahlman (1980) and the contour map shown in Gregory et al. (1983) represent the intensity within the whole energy range 0.1-4.5 keV. Fig. 15 shows examples of X-ray spectra calculated with various column densities of the absorbing gas (Gorenstein and Tucker 1976). This figure teaches us that the knowledge of the X-ray spectrum will be helpful in evaluating the amount of absorption. Recently I obtained the IPC data of the same X-ray observations separated into three energy bands from F. D. Seward of the Smithsonian Astrophysical Observatory. Figs. 16-18 show the X-ray maps in energy bands 0.16-0.81 keV, 0.81-1.73 keV, and 1.73-3.50 keV, which we call L, M, and H, respectively. Fig. 16 shows the presence of the semicircular shell structure clearly. It is naturally explained as enhancement in the plasma density at the outermost part of the SNR interior (see Sedov 1959). We can observe this shell in Fig. 17, but it becomes less prominent in Fig. 18. Since the outermost part of the SNR has the lowest temperature, the X-ray shell is more clearly observed in the lower energy X-ray band. The insufficient

S/N ratio of Fig. 18 also makes features somewhat unclear. However Fig. 18 is also thought to contain the X-ray shell. The CO arm area is a relative depression in all of the three X-ray energy band maps. The X-ray jetlike feature becomes less prominent in Fig. 18. However the CO arm also shows an anticorrelation with the X-ray jetlike feature in Fig. 18 on which the effect of absorption is the smallest. In this map of the energy band H, there is an X-ray hot ridge on the southeast part of the SNR. This hot ridge is observable in the published whole energy range map, but is not so prominent. A mushroom-like feature in Fig. 18 consisting of the X-ray jetlike feature and the southeastern hot ridge seems to have symmetry with respect to the straight line with a position angle of $72^{o}.5$ passing through the X-ray pulsar. For illustrating the X-ray intensity ratio within selected areas, the X-ray color-color diagram seems useful. The areas for plotting are selected as shown in Fig. 19. The resulting color-color diagram is shown in Fig. 20. The error shown in Fig. 20 is roughly determined from the values of the comparison area (C).

V. DISCUSSION

A. The Main Molecular Cloud vs. G109.1-1.0

G109.1-1.0 has a semicircular shape in both of the X-ray and radio continuum emission (Figs. 5 and 6). It is known that the molecular cloud does not absorb the radio continuum emission at all virtually. Therefore the semicircular shape cannot be explained in terms of absorption due to the molecular cloud. The molecular cloud has prevented an isotropic expansion of the SNR resulting in the hemispherical shape. Molecular clouds are probably responsible for various shapes of supernova remnants. However there was only one observational example, the west rim of the Cygnus Loop. In this case the molecular clouds are rather small compared with the SNR. The SNR G109.1-1.0 is the first example of the SNR whose shape has been totally affected by the molecular cloud. The present observations also give direct evidence of the association between G109.1-1.0 and the main molecular cloud.

We consider how much the main molecular cloud has been affected by the SNR in its shape or velocity structure. The SNR shock (blast wave) striking the interstellar cloud will cause two kinds of shocks: the shock propagating into the interstellar cloud (cloud shock) and the shock reflected from the cloud (e. g., McKee and Cowie 1975). The molecular cloud will be affected mainly by the former one. To derive the physical parameters of the cloud shock we must know

those of the blast wave at the time of encounter. The observed X-ray emission from G109.1-1.0 suggests that the eastern part of this SNR is still in the Sedov phase. The evolution of the SNR in the Sedov phase is described in, for example, Sedov (1959), Chevalier (1974), and Spitzer (1978). We assume that the SNR with an initial energy of 1×10^{51} ergs expands in the uniform ambient medium with the hydrogen number density n_H (in cm^{-3}). When t (in yr) has passed since the explosion, the SNR will have the radius r_s, velocity V_s, and postshock temperature T_2 as follows:

$$r_s = 0.31\ t^{2/5}\ n_H^{-1/5}\ pc, \tag{1}$$

$$V_s = 1.2\times10^{5}\ t^{-3/5}\ n_H^{-1/5}\ km\ s^{-1}, \tag{2}$$

$$T_2 = 2.2\times10^{11}\ t^{-6/5}\ n_H^{-2/5}\ K. \tag{3}$$

The radius of G109.1-1.0 is 15' or 18 pc. If we assume n_H = 0.3 cm^{-3}, we obtain an age of 1.4×10^{4} yr, a present shock velocity of 5.1×10^{2} km s^{-1}, and a present postshock temperature of 3.7×10^{6} K. The time when the blast wave struck the main molecular cloud is calculated from the distance of the original cloud surface to the X-ray pulsar or more precisely the explosion site. For simplicity, we assume here that the X-ray pulsar remains at its explosion site, and that the SNR has not changed the shape of the main molecular cloud until now. The separation between the X-ray pulsar and the present surface of the main molecular cloud ranges from 10 pc to 18 pc. The SNR shell reached the

original surface of the main molecular cloud at an SNR age of $0.3\text{-}1.4 \times 10^4$ yr with a shock velocity of $0.5\text{-}1.2 \times 10^3$ km s^{-1}. Using these parameters of the blast wave we derive the parameters of the cloud shock propagating into the cloud. We assume the hydrogen number density of the molecular cloud to be 200 cm^{-3}. The cloud shock is thought to be a radiative shock. This shock has a finite thickness. The temperature of the medium entering the shock front increases abruptly, then decreases gradually due to radiative cooling, and eventually is settled in the equilibrium value. The density increases abruptly up to $\sim 10^3$ cm^{-3} at the shock front as a nonradiative shock, then gradually increases due to radiative cooling in the transition region, and reaches the equilibrium value. We regard a combination of the initial nonradiative shock and the subsequent transition region as one shock front, i. e., the cloud shock. The sound speed C is taken to be the same on both sides of the cloud shock. The ratio of the density behind the cloud shock ρ_{c2} to that ahead it ρ_{c1} is given by

$$\rho_{c2}/\rho_{c1} = V_c^2/C^2, \tag{4}$$

where V_c is the velocity of the cloud shock (Spitzer 1978). The pressure behind the cloud shock is $\rho_{c2}C^2$, and the pressure behind the blast wave is $2\rho_{e1}V_s^2/(\gamma+1)$ where ρ_{e1} is the density ahead of the blast wave and γ is the ratio of specific heats at constant pressure and constant volume.

These two will be of the same order, and using equation (4) we have

$$\rho_{c1} V_c^2 \sim \rho_{e1} V_s^2 \qquad (5)$$

(Spitzer 1978). The derived value of V_c is of order 20-50 km s^{-1}, and it has proceeded by 0-0.5 pc. The value < 0.5 pc is very small compared with the size of the main molecular cloud. The main molecular cloud has not changed the shape of the SNR appreciably after the explosion as assumed above. Therefore the western concave boundary of the main molecular cloud is original or had been made by the stellar wind from the progenitor before the SN explosion. The density ratio ρ_{c2}/ρ_{c1} is estimated to be of order 10^4 from equation (4), and the hydrogen number density behind the cloud shock ρ_{c2} is of order 10^6 cm^{-3}. The cooling time corresponding to the density just behind the initial nonradiative shock of the cloud shock $\sim 10^3$ cm^{-3} is derived to be $\sim$ 300 yr, and the temperature of the matter traveling in the cloud shock will reach its equilibrium within 10^{-2} pc (see Spitzer 1978). The cloud shock will be followed by the high density region with a hydrogen number density of $\sim 10^6$ cm^{-3}. The thickness of this following region must be much less than 10^{-2} pc, because the cloud shock have proceeded only by < 0.5 pc. Thus the thickness of the compressed layer consisting of the cloud shock and the following high density region will be less than 10^{-2} pc. Our observations show that there is no CO enhancement along the interface with the SNR. It may be explained in terms of two reasons. First, the thickness of

compressed postshock layer is less than 1" and cannot be resolved even in the 45 m telescope observations. Second, CO molecules are thought to be fully dissociated in the postshock region in contrast with the case of IC 443, because there is no evidence for the CO emission with a large linewidth of order 20-50 km s^{-1}. It is noteworthy that the value 20-50 km s^{-1} is critical for dissociation of molecules (e. g., Hollenbach and McKee 1980).

Expansions of supernova remnants inside or near molecular clouds were theoretically studied on the basis of hydrodynamical calculations by Tenorio-Tagle, Bodenheimer, and Yorke (1985). Their results for a supernova remnant which has exploded slightly outside the wall of the molecular cloud (Fig. 21) are similar to the appearance of G109.1-1.0, although parameters employed by them are not exactly equal to those of G109.1-1.0. On the other hand, they themselves have pointed out that the X-ray distribution of G109.1-1.0 is similar to the numerical results for the case that the SNR exploded inside the molecular cloud. Sofue, Takahara, and Hirabayashi (1983) and Hughes et al. (1984) claimed that the center of the curvature of the radio shell does not coincide the position of the X-ray pulsar. Our observations indicate that both of the X-ray pulsar and the center of the curvature of the SNR shell are located outside the main molecular cloud. Therefore we conclude that the site of the SN explosion was located outside the main molecular cloud.

B. Effect of Absorption by the CO Arm on the X-Ray Maps

It is interesting to think what the X-ray jetlike feature emerging from the X-ray pulsar represents. The molecular cloud can absorb the X-ray emission. Therefore it is possible that absorption has influence on the appearance of the X-ray image. If the CO arm exists in front of X-ray emitting gas of G109.1-1.0, it will make a depression in the X-ray intensity distribution. To appreciate the effect of absorption we compare the X-ray colors toward the CO arm area with those of the comparison area (C) (Figs. 19 and 20). If the CO arm absorbs a part of the X-ray emission, the X-ray color of the CO arm area becomes harder than that of the comparison area. The straight filament has an H_2 column density $N(H_2)$ of $8\text{-}10 \times 10^{20}$ cm $^{-2}$, and $N(H_2)$ of the curled filament is $1\text{-}2 \times 10^{20}$ cm^{-2}. The cross section normalized per atomic hydrogen as a function of the energy of X-rays is given by Ryter, Cesarsky, and Audouze (1975). Thus we obtain the optical depth for X-rays by multiplying the cross section by the column density. The expected shift due to absorption is given by the arrow with the H_2 column density value of the absorbing gas in Fig. 20. However, Fig. 20 shows that the CO arm has almost the same X-ray color as the comparison area. Toward the CO arm (P, N, and S), the H_2 column density of the molecular gas in front of the X-ray emitting gas is probably less than 2×10^{20} cm^{-2}. We conclude that the X-ray absorption by the CO arm has no effect on the X-ray map. The peak (P) and the straight filament (N) are found to be located behind almost all of or all of the hot

plasma. On the other hand, the location of the curled filament cannot be determined from the X-ray color, because the expected shift corresponding to the H_2 column density of this filament is comparable to the error. However, the curled filament is not so far from the straight one, because these two filaments have the common top and root. Tatematsu et al. (1985) previously pointed out a possibility that the CO arm is located just behind the SNR. They argued that the velocity structure of the CO arm observed with the Nagoya 4 m radio telescope may represent a dynamical effect by the expanding SNR shell. Now we know this velocity structure shows that of the straight CO filament. The kinematics of the CO arm (two CO filaments) are discussed in the next subsection C.

Absorption of the X-ray emission by the molecular cloud is not important in G109.1-1.0. Furthermore, the temperature variation in the SNR seems not to be related to the X-ray jetlike feature, because each of the three energy divided maps (Figs. 16-18) shows the X-ray jetlike feature and because the X-ray colors of this feature and the CO arm are almost equal. Thus, the X-ray images mainly represent the density distribution or more precisely emission measure (the square of electron density integrated along the line of sight) distribution of the hot plasma in G109.1-1.0.

C. Kinematics of the CO Arm

The CO filaments must be closely related to each other,

because they have the common top and root. A natural interpretation is that they form a kind of the molecular loop. Is the velocity difference of the two CO filaments due to dynamical effect of the SNR? We can also apply the discussion for the main molecular cloud to this case. The SNR shell struck the straight filament recently, because the straight filament is located near the rear SNR shell. If the SNR shell struck the CO arm at an SNR age of 1×10^{4} yr, the velocity of the cloud shock is of order 20 km s^{-1}. The shocked molecules are thought to be fully dissociated, because no broad CO emission has been observed toward the CO arm. The velocity difference of the two CO filaments, 2 km s^{-1}, is much smaller than the expected velocity if they are accelerated by the shock wave. The two CO filaments should have survived in the SNR until now. The cloud shock with a velocity of order 20 km s^{-1} proceeds by $\sim$ 0.1 pc from the cloud surface. On the other hand, the linear widths of the filaments are $\sim$ 2 pc. The thin surface layer of the original CO filaments has been shocked. Therefore the shape and velocity structure of the CO filaments have been unchanged since the SN explosion. There is a possibility that the shape and velocity structure are a result of the effect by the stellar wind from the progenitor. We wonder what the abrupt velocity change seen in Fig. 13 means. One may interpret it as a kind of dynamical acceleration by the SNR. However the small difference in velocity and the observed line shape probably prefer the origin other than the dynamical effect by the SNR. We suggest that it represents a part of the western half of the straight

filament seen in V_{LSR} = (-49, -45) km s^{-1}.

D. The X-ray Jetlike Feature

The clear anticorrelation may imply the close relationship between the CO arm and the X-ray jetlike feature. However it is strange that the outer boundary of the CO arm seems not to delineate the inner boundary of the X-ray jetlike feature perfectly (Fig. 10). In particular, there is an apparent gap between the X-ray pulsar and the curled X-ray feature (Gregory and Fahlman 1983). Now we know that the X-ray jetlike feature represents the density enhancement of the plasma. It is interesting to think whether the CO arm is related to the plasma enhancement seen as the X-ray jetlike feature or not. How much does the X-ray shell contribute to the shape of the X-ray jetlike feature. To some degree it must contribute, because the northern part of the X-ray jetlike feature cannot be discerned from the X-ray shell. It is interesting that the northern part of the X-ray shell, which is a part of the X-ray jetlike feature, seems intenser than the remainder of the X-ray shell. We will try to interpret the X-ray jetlike feature in terms of a combination of the northern part of the X-ray shell and an additional X-ray feature located between the X-ray pulsar and the shell. The shape of the additional feature is not well known. In Fig. 16 the X-ray blob located 8' east of the X-ray pulsar looks isolated, whereas in Fig. 18 the X-ray ridge seems to be smoothly connected from the X-ray pulsar

to the X-ray shell. We will discuss three possible explanations for the formation of the X-ray jetlike feature.

First, we discuss the case that the diffuse envelope of the CO arm has contributed to the formation. We may assume that two CO filaments had a diffuse envelope consisting of atomic gas. This assumption may be justified by the observational evidence that in some regions the molecular cloud is embedded in the HI cloud: e. g., the Mon OB1 and Mon OB2 molecular clouds (Blitz 1978). The envelope would be heated up by the blast wave of the SNR. The shocked envelope will become an additional X-ray emitting hot gas, and be seen as the X-ray jetlike feature. Tatematsu et al. (1985) have shown that the main molecular cloud accompanies an HI cloud. The higher density of the envelope around the main molecular cloud may result in the absence of X-ray enhancement at the interface between the SNR and the main molecular cloud at R. A. = 22^h58^m, because the temperature of the shocked gas becomes lower. The envelope of the CO arm is assumed to have a moderate density such that the postshock temperature remains higher than 10^6 K and that a postshock gas of this envelope has a sufficient density-contrast to the plasma in the cloud-free region. The former condition is translated into the preshock density condition by using equation (3). The postshock temperature higher than 10^6 K is accomplished if the hydrogen number density of the envelope is less than $\sim$ 10 cm^{-3}. The bright-rimmed CO arm in the X-ray emission along with the northern X-ray shell can be observed as the X-ray jetlike feature. The separation between the X-ray jetlike feature and the CO arm can be made

in some appropriate density distribution of the envelope.

Second, we discuss the case that the main molecular cloud on the west has mainly contributed to the formation of the X-ray jetlike feature. Fig. 21 shows the results of a calculation for the SNR expanding in the vicinity of the wall of the molecular cloud by Tenorio-Tagle, Bodenheimer, and Yorke (1985). This calculation contains the effect of radiative cooling. We can observe an emission measure structure like a mushroom (a semicircular shell and a stem), although the limitation of calculated points makes the resulting structure somewhat unclear. The stem of a mushroom is formed as follows; the shock reflected by the main molecular cloud causes a strong compression of the plasma particularly between the X-ray pulsar and the cloud, the denser plasma between them is then cooled by radiation, and the hot plasma flows into the stem due to the pressure gradient. This structure resembles that in the map of the energy band H (Fig. 18). The stem along with the northern X-ray shell can be seen as the X-ray jetlike feature. A part of the stem close to the molecular cloud should be strongly cooled due to radiation. The gap between the curled X-ray feature and the X-ray pulsar (or the main molecular cloud) is possibly explained in this way. It is interesting to calculate the X-ray intensity distribution, although they present only the density distribution shown in Fig. 21. A close examination indicates that the symmetry axis in Fig. 18 is not exactly perpendicular to the contact surface with the main molecular cloud. We must note that the CO arm was

not involved in their calculation. It seems possible that the effect of the CO arm makes the result of the calculation more similar to the observed structure. Such calculations are highly desirable.

Third, we discuss the case that neither of the main molecular cloud nor the CO arm is related to the density enhancement of the plasma. In this case the apparent anticorrelation is thought to be observed by chance. It seems also natural to interpret the X-ray map as a composite of the ordinary shell structure and an additional hot blob. The blob is located on the east of the X-ray pulsar. The separation between the X-ray pulsar and this blob becomes smaller with increasing X-ray energy (Figs. 16-18). It seems also possible to interpret this blob as a kind of the jet ejected from the X-ray pulsar. The two X-ray lobes on opposite sides of SS 433 are thought to be jets ejected from it (Seward et al. 1980). The hot blob along with the northern X-ray shell can be observed as the X-ray jetlike feature.

We have discussed three possible explanations for the density enhancement corresponding to the X-ray jetlike feature. In order to establish the conclusive model for the X-ray jetlike feature, we need new X-ray observations with a higher angular-resolution.

E. The Energy of G109.1-1.0 and Influence on the Molecular Cloud

We summarize the relationship of these two objects, the

SNR and the molecular cloud. The cloud shock has a velocity of 20-50 km s^{-1}. This value is comparable to the critical value of the shock velocity for the dissociation of molecules (Hollenbach and McKee 1980). Our observations shows that the shocked molecules in the G109.1-1.0 region are fully dissociated. The energy used for dissociation is probably within the same order of the kinetic energy of the cloud shock. The cloud shock proceeds by < 0.5 pc from the original surface of the molecular cloud. The thickness of the postshock layer is probably less than 10^{-2} pc. The postshock temperature of the cloud shock is < 10^{6} K because of the higher density of the molecular cloud, and the shock is radiative. The appreciable part of the SNR energy is thought to be radiated. The western part of the SNR entered the radiative phase much earlier than the eastern half. The momentum of the cloud shock conserves approximately. The thickness of the shocked layer is much smaller than the size of the molecular cloud. However the momentum of the cloud shock appreciably affects the main molecular cloud in 10^{5}-10^{6} yr. On the other hand, the dynamical effect on the molecular cloud will be much less if the very old SNR with an age of 10^{5}-10^{6} yr strikes the molecular cloud for the first time. The expansion velocity of the blast wave decreases with increasing age, and equation (5) indicates that the resulting cloud shock velocity also decreases. Therefore the molecular cloud will be affected if it is struck by the SNR whose age is not very old. The shell of G109.1-1.0 struck the main molecular cloud at an SNR age of

5×10^3 yr for the first time. The dynamical effect of G109.1-1.0 now stored in the very thin layer will compress the molecular cloud in the future.

The reflected shock returns the energy into the SNR interior and will affect of the evolution of this SNR. If the reflected shock is dense enough to suffer radiative cooling, it will let the SNR energy escape. The interpretation of the X-ray jetlike feature in terms of the reflected shock (see the preceding subsection D.) will lead to radiative loss due to the reflected shock. Now we cannot estimate the amount of radiative loss due to the reflected shock from the observational data, because we have no numerical calculation detailed enough to compare with the observed X-ray intensity distribution.

Although we have no direct information on the energy transfer related to G109.1-1.0, we try to make rough estimation on the order of various kinds of energy. Half of the total energy of the SNR corresponding to the western hemisphere, 5×10^{50} ergs, has been related to the main molecular cloud. It was used for the cloud shock, reflected shock, dissociation of molecules, and radiation. If the cloud shock propagating into the main molecular cloud has a velocity of 30 km s^{-1}, it has a kinetic energy of order 2×10^{49} ergs. The energy used for dissociation of the molecules in the main molecular cloud probably is in the same order. It is difficult to expect the value of the energy of the shock reflected by the main molecular cloud. If it is the same order as the kinetic energy of the cloud shock, the energy radiated from the main molecular cloud

will be $\sim 4.3\times10^{50}$ ergs. Therefore most of the energy of the western half of G109.1-1.0 has been radiated. The other half of the initial SNR energy nearly conserves in the eastern half of the SNR. However the interaction with the molecular cloud may affect also the eastern half of the SNR. The energy $\sim 2\times10^{49}$ ergs was radiated due to the interaction with the CO arm. The CO arm may have obtained $\sim 3\times10^{47}$ ergs as the energy of cloud shock and the energy of the same order as the dissociation of molecules. The reflected shock from both of the main molecular cloud and CO arm also affects the evolution of the SNR. The momentum deposited in the main molecular cloud is of order 6×10^{4} $M_{\odot}$ km s^{-1}, and that of the CO arm is of order 2×10^{3} $M_{\odot}$ km s^{-1}. They will affect the shape and kinematics of the molecular cloud in the future.

F. A CO Survey of the Interaction

The successful observations of G109.1-1.0 led us to a survey project for the evidence of the interaction between the SNR and the molecular cloud. It is in progress on the Nagoya 4 m radio telescope. The purposes of this survey are to obtain other convincing observational examples and to derive the percentage of supernova remnants accompanying molecular clouds. The number of SNRs in the Galaxy is about 150. The typical size of nearby SNRs (within 4 kpc from the sun) is $30'-3^{\circ}$, very large compared with the beamsize of the 4 m radio telescope, 2'.7. Therefore it is difficult to survey all the SNRs fully. To avoid the confusion of unrelated cloud, we mainly choose the SNRs located in the outer Galaxy (where the galactocentric distance is larger than 10 kpc). Huang (1985) has already surveyed the CO gas toward such SNRs within the galactic longitudal range $l = 70^{\circ}-210^{\circ}$ using the Columbia 1.2 m radio telescope. The resolution of his survey, $8'-1^{\circ}$, is too coarse to investigate the association of the CO cloud with the SNR or to obtain the evidence of the interaction. However this survey will serve as a good basis for our survey of the interaction. We can omit observations of the SNRs toward which he has not detected the CO cloud having a possibility of the association. I plan to finish this survey in two more years.

VI. SUMMARY

The unusual semicircular supernova remnant G109.1-1.0 has been observed in the J = 1-0 transitions of CO and ^{13}CO. The Nagoya 4 m radio telescope and the Nobeyama 45 m radio telescope were used for the observations. The molecular cloud on the west of G109.1-1.0 is found to be in contact with this remnant. This is the first observational evidence of the supernova remnant expanding in the vicinity of the wall of the molecular cloud. There is a molecular ridge (CO arm) extending from the main body of the molecular cloud toward the east. The CO arm consists of two remarkably thin CO filaments with sizes of 2 pc × 18 pc. These two filaments have the common top and root. The only thin (less than $\sim$ 0.5 pc) surface layer of the molecular cloud in contact with G109.1-1.0 may have been shocked, and molecules in this layer are thought to be fully dissociated. Although the compression layer is not observed at present, the momentum deposited in the cloud shock must result in the compression of the molecular cloud in the future (in 10^5-10^6 yr). The CO arm shows an apparent anticorrelation with the X-ray jetlike feature in G109.1-1.0. The X-ray color does not show evidence of the X-ray absorption by the CO arm. One of the CO filaments is found to be located near the rear SNR shell. The X-ray jetlike feature may represent the enhancement in density surrounding the CO arm. We discuss three possible explanations for the formation of the X-ray

jetlike feature. First, the diffuse envelope surrounding the CO arm has been shocked by the blast wave, and the CO arm becomes bright-rimmed. Second, the SNR shock reflected by the main molecular cloud causes a mushroom-like structure of the hot plasma in the SNR, and a part of this feature is observed as the X-ray jetlike feature. In this case the CO arm may also contribute to the formation of the observed X-ray feature additionally. Third, the hot plasma blob ejected from the X-ray pulsar and the X-ray shell have formed the X-ray jetlike feature, and the anticorrelation between the CO arm and the X-ray jetlike feature is chance coincidence. We can select the conclusive model from them if we obtain higher angular-resolution X-ray maps. The former two explanations indicate the possibility that the influence of the molecular cloud has contributed to the formation of this feature. The present observations unambiguously established that G109.1-1.0 is associated with the molecular cloud and suggest that they have interacted with each other.

APPENDIX A. ESTIMATION OF COLUMN DENSITY AND MASS

There are a few methods to estimate the mass of the molecular cloud. The most popular way is to calculate through the ^{13}CO column density assuming local thermodynamic equilibrium (LTE). The terrestrial abundance ratio of CO/^{13}CO is 89, whereas the intensity ratio of CO/^{13}CO observed toward the molecular cloud ranges 1-10. Therefore CO is thought to be optically thick. We assume the same excitation temperature T_{ex} for both of CO and ^{13}CO. Observed specific intensity is expressed as

$$I_\nu = [B_\nu(T_{ex})-B_\nu(2.7\ \mathrm{K})][1-\exp(-\tau)], \qquad \text{(A1)}$$

where B_ν is the Planck function and τ is the optical depth of an observed line. The value of T_{ex} is deduced from the observed CO intensity, because the optical depth of CO is thought to be much larger than unity and the term $\exp(-\tau)$ for CO is negligible. From T_{ex} and the observed ^{13}CO intensity, we obtain the ^{13}CO optical depth, τ_{13}. When we assume LTE, the ^{13}CO column density N_{13} is given by

$$N_{13} = [3kT_{ex}\tau_{13}\Delta V_{13}]/[4\pi^3\mu^2\nu_{13}\{1-\exp(-h\nu_{13}/kT_{ex})\}]. \qquad \text{(A2)}$$

Here ΔV_{13} is the full width at half maximum of the ^{13}CO emission profile, μ is the electric dipole moment of the CO molecule, k is Boltzmann's constant, and h is Planck's constant. Dickman (1978) obtained the ^{13}CO column density

toward molecular clouds with a visual extinction A_V of 1.5 - 10 mag, and compared it with the hydrogen column density. According to him the conversion factor from ^{13}CO column density N_{13} to H_2 column density is $(5.0 \pm 2.5) \times 10^5$. We integrate the H_2 column density over the area of the molecular cloud to obtain the number of H_2 molecules. Assuming a mean molecular weight of 2.76 m_H per H_2 molecule, we obtain the mass of the molecular cloud. This LTE mass is believed to be accurate within a factor of 2.

REFERENCES

Blair, W. P., and Kirshner, R. P. 1981, Nature, 291, 132.

Blitz, L. 1978, Ph. D. thesis, Columbia University.

Chevalier, R. A. 1974, Ap. J., 188, 501.

Dame, T. M. 1983, Ph. D. thesis, Columbia University.

Davis, J. G., Lyne, A. G., and Seiradakis, J. H. 1972, Nature, 240, 229.

Davis, J. H., and Vanden Bout, P. 1973, Ap. Letters, 15, 43.

DeNoyer, L. K. 1979, Ap. J. (Letters), 232, L165.

DeNoyer, L. K., and Frerking, M. A. 1981, Ap. J. (Letters), 246, L37.

Dickman, R. L. 1978, Ap. J. Suppl., 37, 407.

Downes, A. 1983, M. N. R. A. S., 203, 695.

Fahlman, G. G., and Gregory, P. C. 1981, Nature, 293, 202.

---. 1983, in IAU Symposium 101, Supernova Remnants and Their X-Ray Emission, ed. J. Danziger and P. Gorenstein (Dordrecht: Reidel), p. 445.

Fukui, Y., and Tatematsu, K. 1987, in IAU Colloquium 101, Supernova Remnants and the Interstellar Medium, (Cambridge: Cambridge University Press), p. 261.

Giacconi, R., et al. 1979, Ap. J. 230, 540.

Gorenstein, P., and Tucker, W. H. 1976, Ann. Rev. Astr. Ap., 14, 373.

Gregory, P. C., Braun, R., Fahlman, G. G., and Gull, S. F. 1983, in IAU Symposium 101, Supernova Remnants and Their X-Ray Emission, ed. J. Danziger and P. Gorenstein (Dordrecht: Reidel), p. 437.

Gregory, P. C., and Fahlman, G. G. 1980, Nature, 278, 805.

---. 1981, Vistas Astr., 25, 119.

---. 1983, in IAU Symposium 101, Supernova Remnants and Their X-Ray Emission, ed. J. Danziger and P. Gorenstein (Dordrecht: Reidel), p. 429.

Grindlay, J. E., Band, D., Seward, F., Leahy, D., Weisskopf, M. C., and Marshall, F. E. 1984, Ap. J., 277, 286.

Heiles, C. 1987, Ap. J., 315, 555.

Heydari-Malayeri, M., Kahane, C., and Lucas, R. 1981, Nature, 293, 549.

Hollenbach, D., and McKee, C. F. 1980, Ap. J. (Letters), 241, L47.

Huang, Y.-L. 1985, Ph. D. thesis, Columbia University.

Huang, Y.-L., Dame, T. M., and Thaddeus, P. 1983, Ap. J., 272, 609.

Huang, Y.-L., Dickman, R. L., and Snell, R. L. 1986, Ap. J. (Letters), 302, L63.

Hughes, V. A., Harten, R. H., Costain, C. H., Nelson, L. A., and Viner, M. R. 1984, Ap. J., 283, 147.

Hughes, V. A., Harten, R. H., and van den Bergh, S. 1981 Ap. J. (Letters), 246, L127.

Israel, F.P. 1980, A. J., 85, 1612.

Kawabata, K., Ogawa, H., Fukui, Y., Takano, T., Fujimoto, Y., Kawabe, R., Sugitani, K., and Takaba, H. 1985, Astr. Ap., 151, 1.

Koyama, K., Hoshi, R., and Nagase, F. 1987, Pub. Astr. Soc. Japan, 39, 801.

Kutner, M. L., and Ulich, B. L. 1981, Ap. J., 250, 341.

Manchester, R. N., and Taylor, J. H. 1981, A. J., 86, 1953.

McKee, C. F., and Cowie, L. L. 1975, Ap. J., 195, 715.

Middleditch, J., Pennypacker, C. R., and Burns, M. S. 1983, Ap. J., 274, 313.

Öpik, E. J. 1953, Irish Astr. J., 2, 219.

Penzias, A. A., and Burrus, C. A. 1973, Ann. Rev. Astr. Ap., 11, 51.

Ryter, C., Cesarsky, C. J., and Audouze, J. 1975, Ap. J., 198, 103.

Scoville, N. Z., Irvine, W. M., Wannier, P. G., and Predmore, C. R. 1977, Ap. J., 216, 320.

Sedov, L. I. 1959, Similarity and Dimensional Methods in Mechanics (translated from the Russian edition by M. Friedman) (New York: Academic Press).

Seward, F., Grindlay, J. E., Seaquist, E., and Gilmore, W. 1980, Nature, 287, 806.

Sharpless, S. 1959, Ap. J. Suppl., 4, 257.

Sofue, Y., Takahara, F., and Hirabayashi, H. 1983, Pub. Astr. Soc. Japan, 35, 447.

Spitzer, L., Jr. 1978, Physical Processes in the Interstellar Medium (New York: John Wiley & Sons).

Takano, T., Ogawa, H., Kato, T., Fujimoto, M., Fujimoto, Y., Fukui, Y., Hayashi, Y., Kawabata, K., Kawabe, R., and Sofue, Y. 1983, Pub. Astr. Soc. Japan, 35, 323.

Tatematsu, K., Fukui, Y., Iwata, T., and Nakano, M. 1987, Pub. Astr. Soc. Japan, 39, 755.

Tatematsu, K., Nakano, M., Yoshida, S., Wiramihardja, S. D., and Kogure, T. 1985, Pub. Astr. Soc. Japan, 37, 345.

Tenorio-Tagle, G., Bodenheimer, P., and Yorke, H. W. 1985,

Astr. Ap., 145, 70.

Tomisaka, K., and Ikeuchi, S. 1986, Pub. Astr. Soc. Japan, 38, 697.

Weiler, K. W. 1985, in The Crab Nebula and Related Supernova Remnants, ed. M. C. Kafatos and R. B. C. Henry (Cambridge: Cambridge University Press), p. 227.

White, G. J., Rainey, R., Hayashi, S. S., and Kaifu, N. 1987, Astr. Ap., 173, 337.

Wootten, H. A. 1977, Ap. J., 216, 440.

Wootten, A. 1981, Ap. J., 245, 105.

FIGURE LEGENDS

Fig. 1. --- The 0.1-4.5 keV X-ray map of G109.1-1.0 is reproduced from Gregory et al. (1983). The resolution of this map is 2'.5. Contours are drawn at levels of 20, 30, 40, 52, 67, 83, 100, 118, 142, 200, 332, 470, 664, 940, 1328, and 1878 in an arbitrary unit.

Fig. 2. --- The 10 GHz continuum map of G109.1-1.0 obtained by Sofue et al. (1983) is shown. The resolution of this map is 2'.7. The lowest contour level is 11.02 mK, and the contour interval is 5.51 mK.

Fig. 3. --- The overall structure of the molecular cloud obtained in our previous CO observations with the Nagoya 4 m radio telescope (Tatematsu et al. 1985). The contours of the CO (J = 1-0) emission at levels of T_A^* = 5.5, 8.0, 10.0, 15.0, and 20.0 K are shown as solid lines. The dash-dotted lines show the 10 GHz image of G109.1-1.0 (Sofue et al. 1983). The X-ray jetlike feature is shaded. The Greek letters represent CO intensity maxima.

Fig. 4. --- The map of the CO (J = 1-0) intensity integrated over the range of V_{LSR} = (-55, -45) km s^{-1} obtained with the Nagoya 4 m radio telescope. Observed points are illustrated as filled circles and filled triangles. Toward the direction of the filled triangles ^{13}CO spectra were obtained besides CO spectra. The contour interval is 7 K km s^{-1}.

Fig. 5. --- The integrated CO intensity map obtained with the Nagoya 4 m radio telescope is superimposed upon the 0.1-4.5 keV X-ray map of G109.1-1.0 by Gregory et al. (1983). The X-ray jetlike feature is shaded.

Fig. 6. --- The integrated CO intensity map obtained with the Nagoya 4 m radio telescope is superimposed upon the 10 GHz continuum map by Sofue et al. (1983).

Fig. 7. --- The profiles in CO and ^{13}CO toward the CO intensity maximum at the top of the CO arm.

Fig. 8. --- The observed area and the employed spacing interval in the observations with the Nobeyama 45 m radio telescope.

Fig. 9. --- The contour map of the CO (J = 1-0) intensity integrated over the radial velocity range V_{LSR} = (-57, -43) km s^{-1} obtained with the Nobeyama 45 m radio telescope. The contour interval is 3.0 K km s^{-1}.

Fig. 10. --- Contours of the CO (J = 1-0) intensity integrated over the range V_{LSR} = (-53, -47) km s^{-1} obtained with the Nobeyama 45 m radio telescope are shown as thick lines. The contour interval is 3.0 K km s^{-1}. The 0.1-4.5 keV X-ray map of G109.1-1.0 (Gregory et al. 1983) is reproduced as thin lines.

Fig. 11. --- The map of CO (J = 1-0) intensity integrated over the range V_{LSR} = (-51, -49) km s^{-1} around the X-ray jetlike feature obtained with the Nobeyama 45 m radio telescope. The contour interval is 1.5 K km s^{-1}. The X-ray map of G109.1-1.0 (Gregory et al. 1983) is also reproduced as thin lines.

Fig. 12. --- The same as Fig. 2 but for the range V_{LSR} = (-49, -47) km s^{-1}.

Fig. 13. --- The CO (J = 1-0) position-velocity diagram along Decl. (1950) = $58^{o}45'30''$ obtained with the Nobeyama 45 m radio telescope. The contour interval is 1.5 K.

Fig. 14. --- The distribution of the column density of hydrogen molecules $N(H_2)$ deduced from the data obtained with the Nagoya 4 m radio telescope. The contour interval is 5 × 10^{20} cm^{-2}. The dashed line illustrates the boundary of the CO arm. The filled triangles represent the positions observed in both of CO and ^{13}CO.

Fig. 15. --- The calculated spectra of the absorbed X-ray emission. The intrinsic spectrum is assumed as dN/dE = 10 E^{-2} photons cm^{-2} s^{-1} keV^{-1}. This is taken from Gorenstein and Tucker (1976).

Fig. 16. --- The map of the X-ray energy band L. The band covers 0.16-0.81 keV. The resolution of the map is $\sim$ 2'.5.

This is obtained from F. D. Seward.

Fig. 17. --- The map of the X-ray energy band M. The band covers 0.81-1.73 keV. This is obtained from F. D. Seward.

Fig. 18. --- The map of the X-ray energy band H. The band covers 1.73-3.50 keV. This is obtained from F. D. Seward.

Fig. 19. --- The areas used for the X-ray color-color diagram (Fig. 20). The contours represent the 0.33-3.50 keV X-ray map which omits the lower and upper ends of the IPC energy range for improving the S/N ratio. This is obtained from F. D. Seward.

Fig. 20. --- The X-ray color-color diagram. The ordinate shows the intensity ratio of the energy band H (1.73-3.50 keV) to the energy band M (0.81-1.73 keV). The abscissa is the intensity ratio of the energy band M to the energy band L (0.16-0.81 keV).

Fig. 21. --- The results of a two-dimensional numerical calculation for the case that a supernova explodes with an initial energy of 10^{51} ergs at a distance of 2 pc from a cylindrical cloud (Tenorio-Tagle, Bodenheimer, and Yorke 1985). The hydrogen number density of the cloud is 10^{3} cm^{-3}, and the intercloud density is 1 cm^{-1}. The panels a, b, c, and d illustrate the shapes of the supernova remnant 100, 3.06×10^{3}, 1.19×10^{4}, and 2.65×10^{4} yr later since the explosion, respectively.

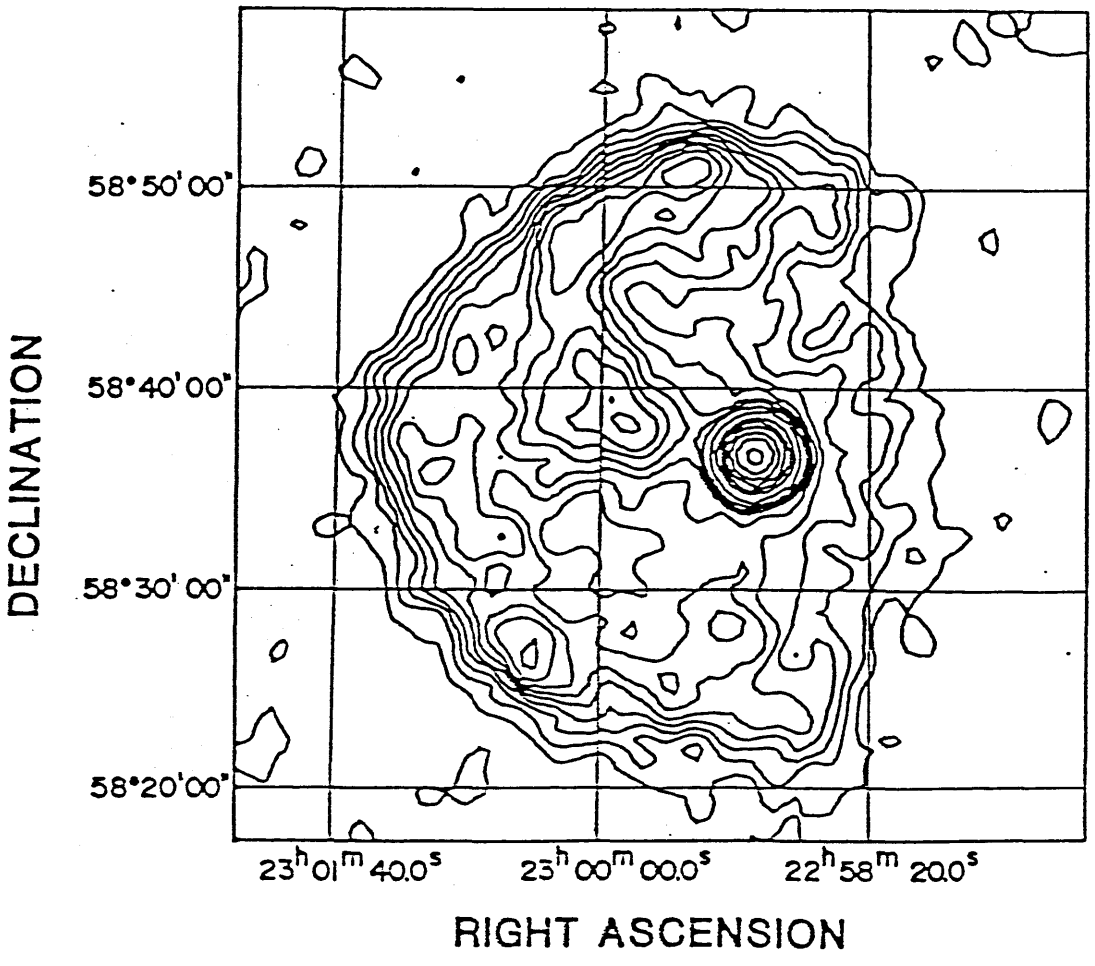
58°50'00"
58°40'00"
58°30'00"
58°20'00"
DECLINATION
23h01m40.0s
23h00m00.0s
22h58m20.0s
RIGHT ASCENSION

Fig. 1.

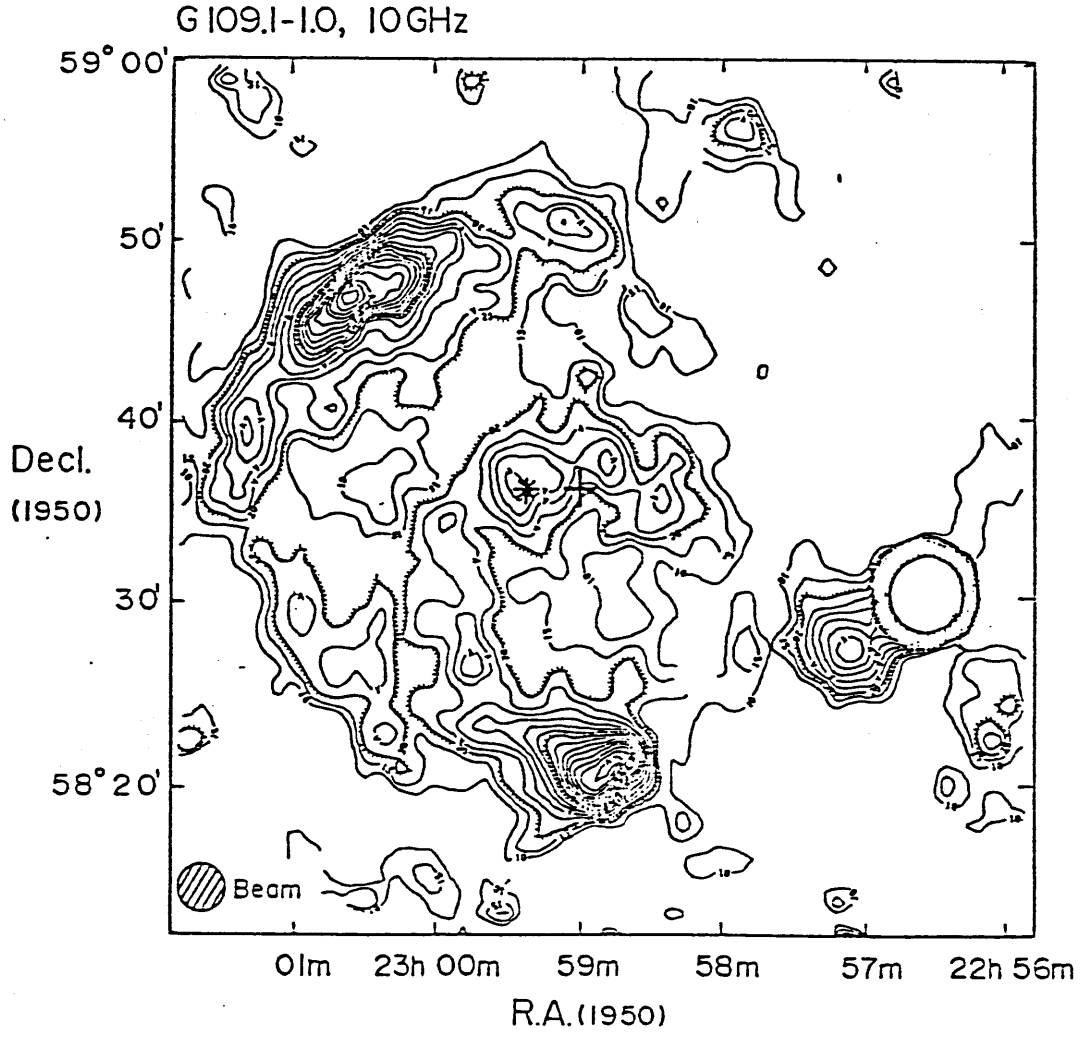
G 109.1-1.0, 10GHz
59° 00'
50'
40'
30'
58° 20'
Decl.
(1950)
Beam
01m
23h 00m
59m
58m
57m
22h 56m
R.A.(1950)

Fig. 2.

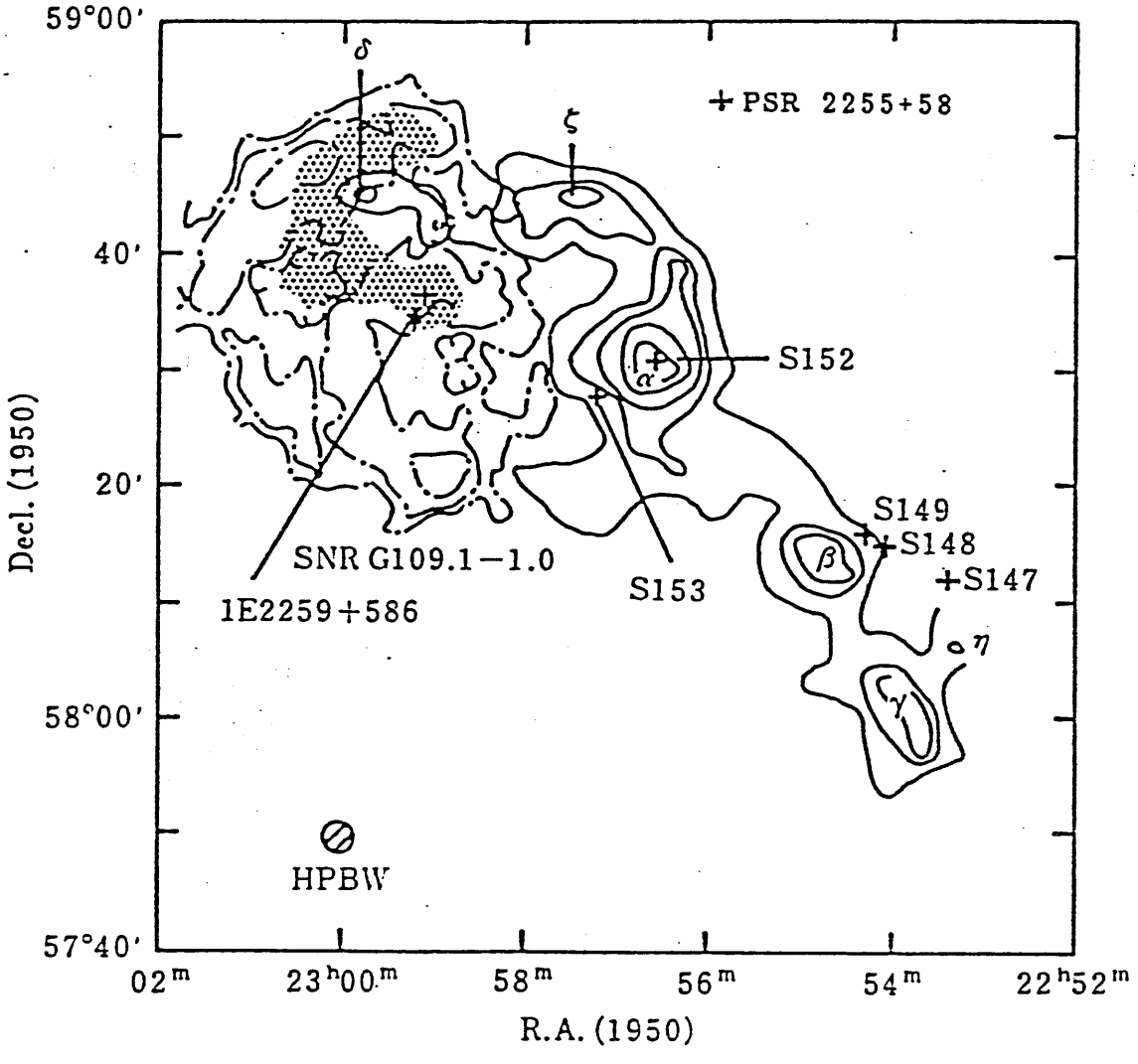
59°00'
40'
20'
58°00'
57°40'
Decl. (1950)
δ
ζ
+PSR 2255+58
S152
S149
+S148
+S147
S153
SNR G109.1−1.0
1E2259+586
η
HPBW
02m
23h00m
58m
56m
54m
22h52m
R.A. (1950)

Fig. 3.

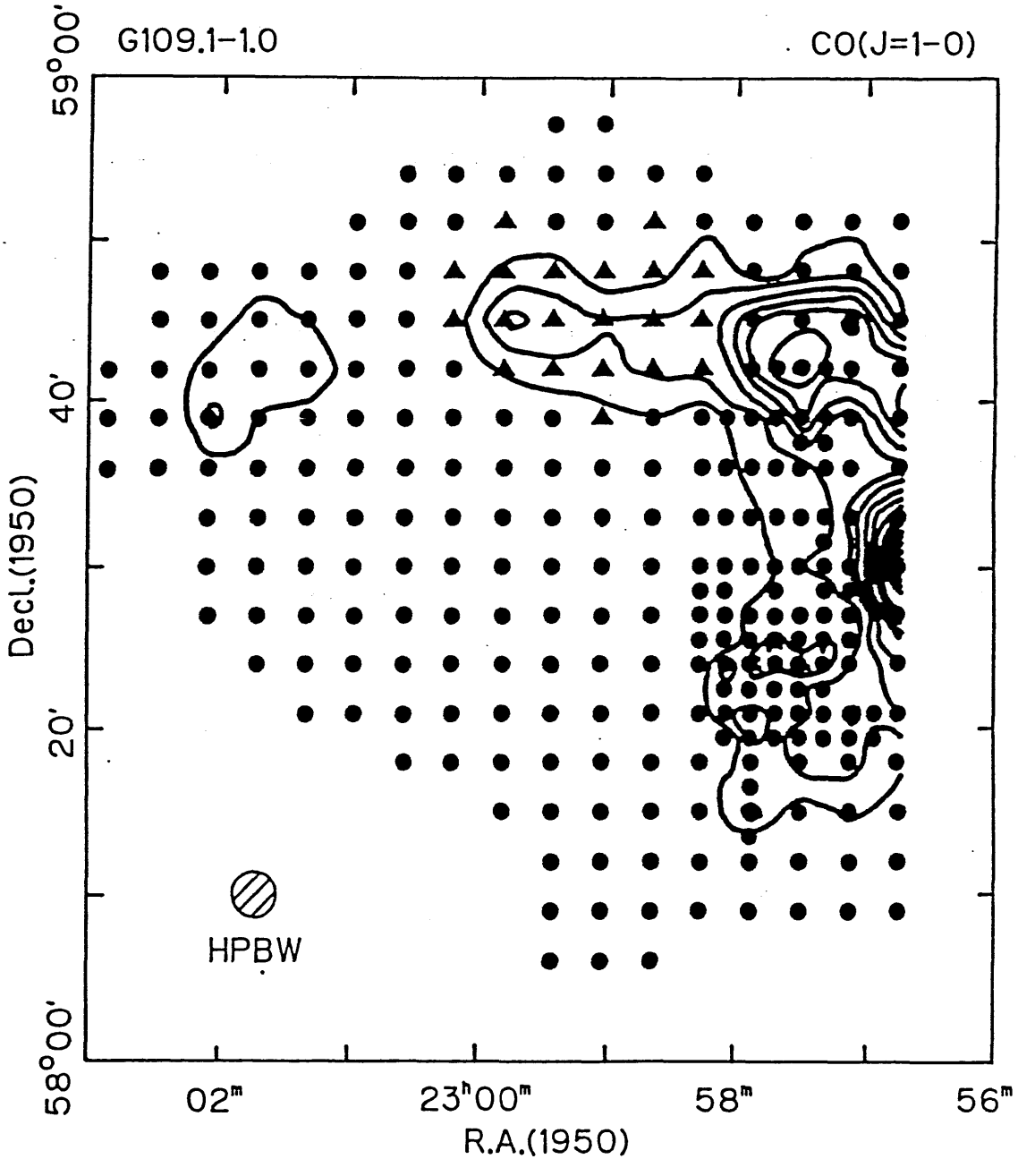
G109.1-1.0
CO(J=1-0)
59°00'
40'
20'
58°00'
Decl.(1950)
HPBW
02ᵐ
23ʰ00ᵐ
58ᵐ
56ᵐ
R.A.(1950)

Fig. 4.

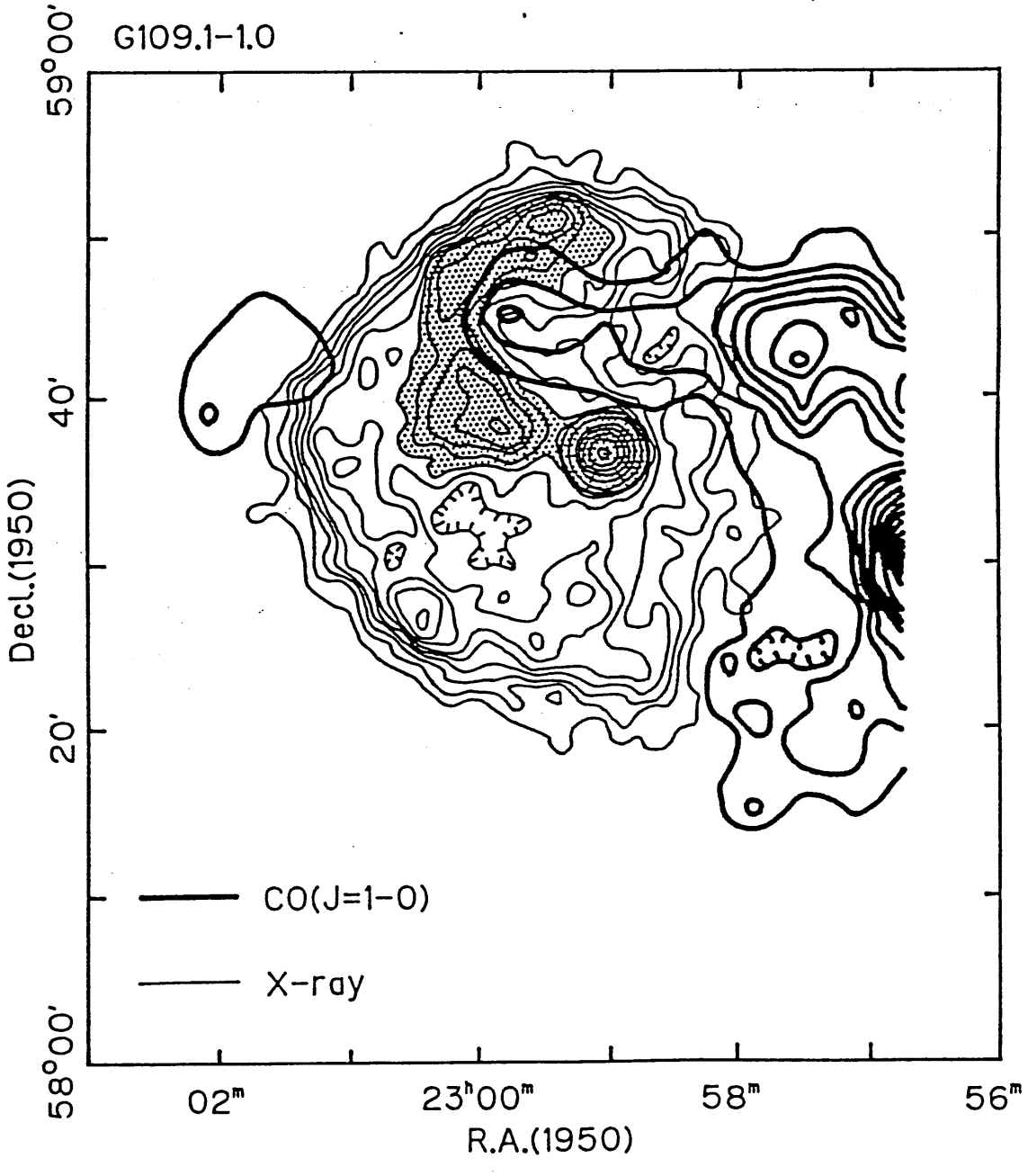
G109.1-1.0
59°00'
40'
20'
58°00'
Decl.(1950)
02ᵐ
23ʰ00ᵐ
58ᵐ
56ᵐ
R.A.(1950)
CO(J=1-0)
X-ray

Fig. 5.

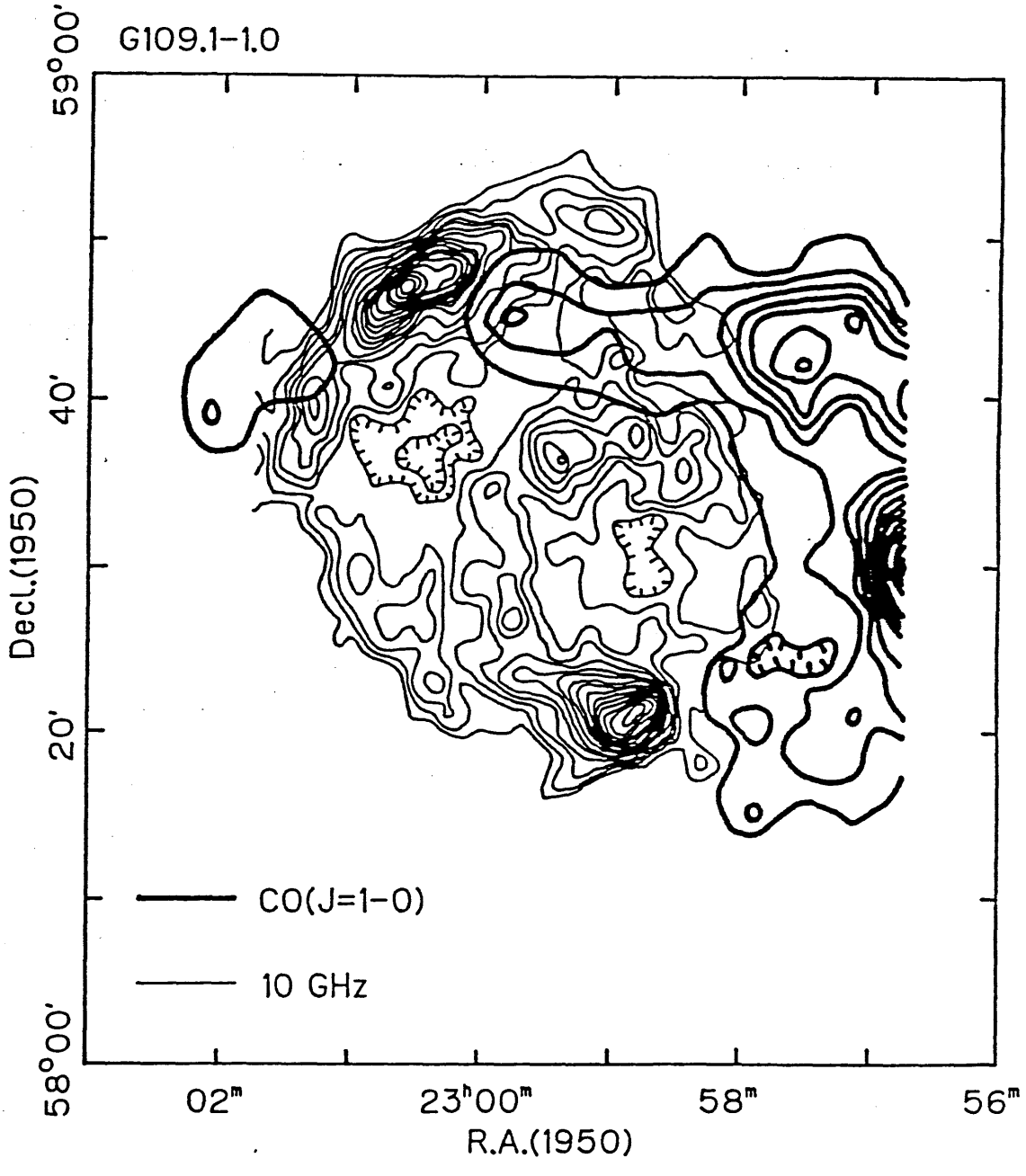
G109.1-1.0
59°00'
40'
20'
58°00'
Decl.(1950)
CO(J=1-0)
10 GHz
02ᵐ
23ʰ00ᵐ
58ᵐ
56ᵐ
R.A.(1950)

Fig. 6.

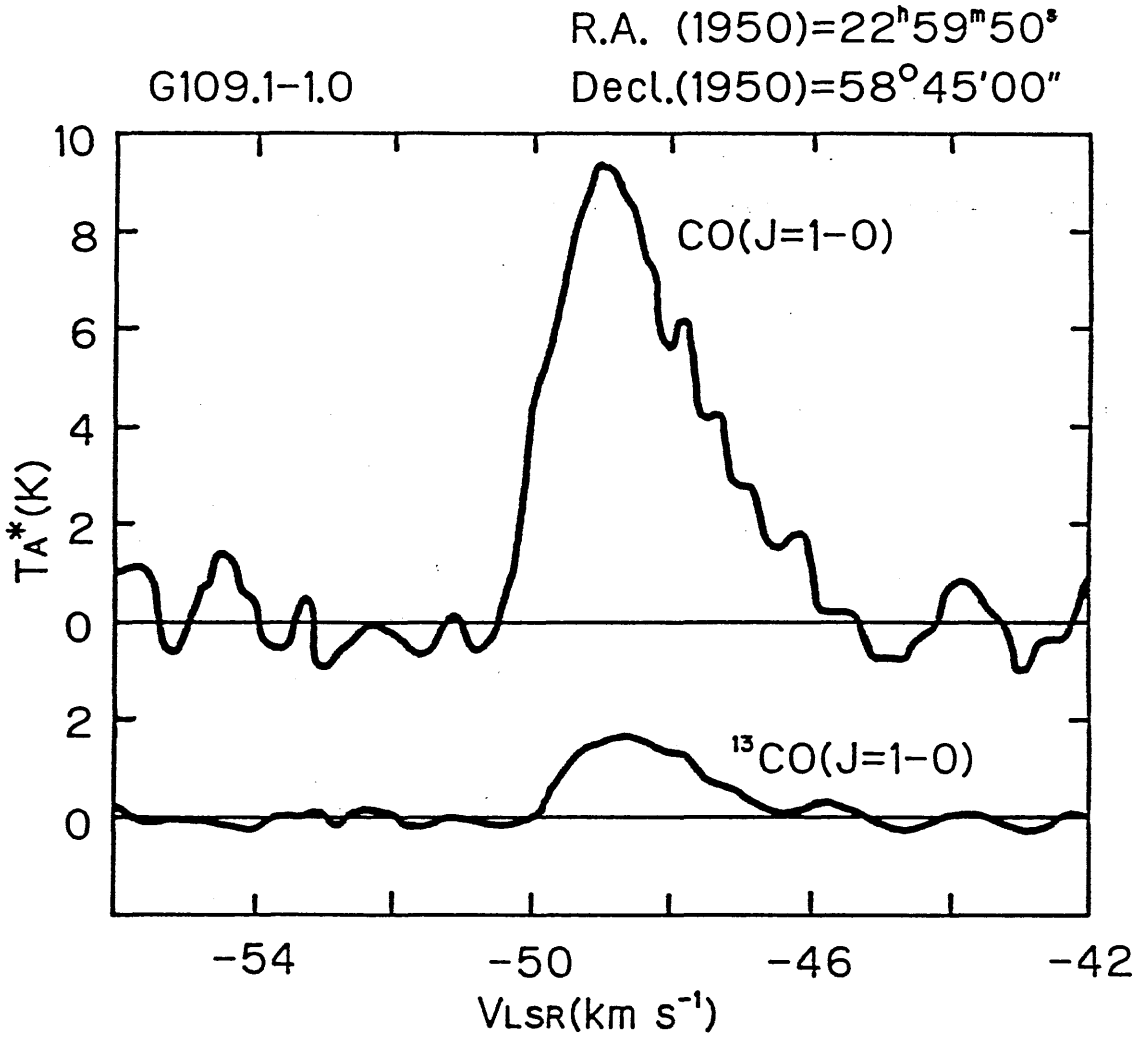
R.A. (1950)=22h59m50s
G109.1-1.0
Decl.(1950)=58°45'00"
10
8
6
4
2
0
2
0
CO(J=1-0)
13CO(J=1-0)
TA*(K)
-54
-50
-46
-42
VLSR(km s-1)

Fig. 7.

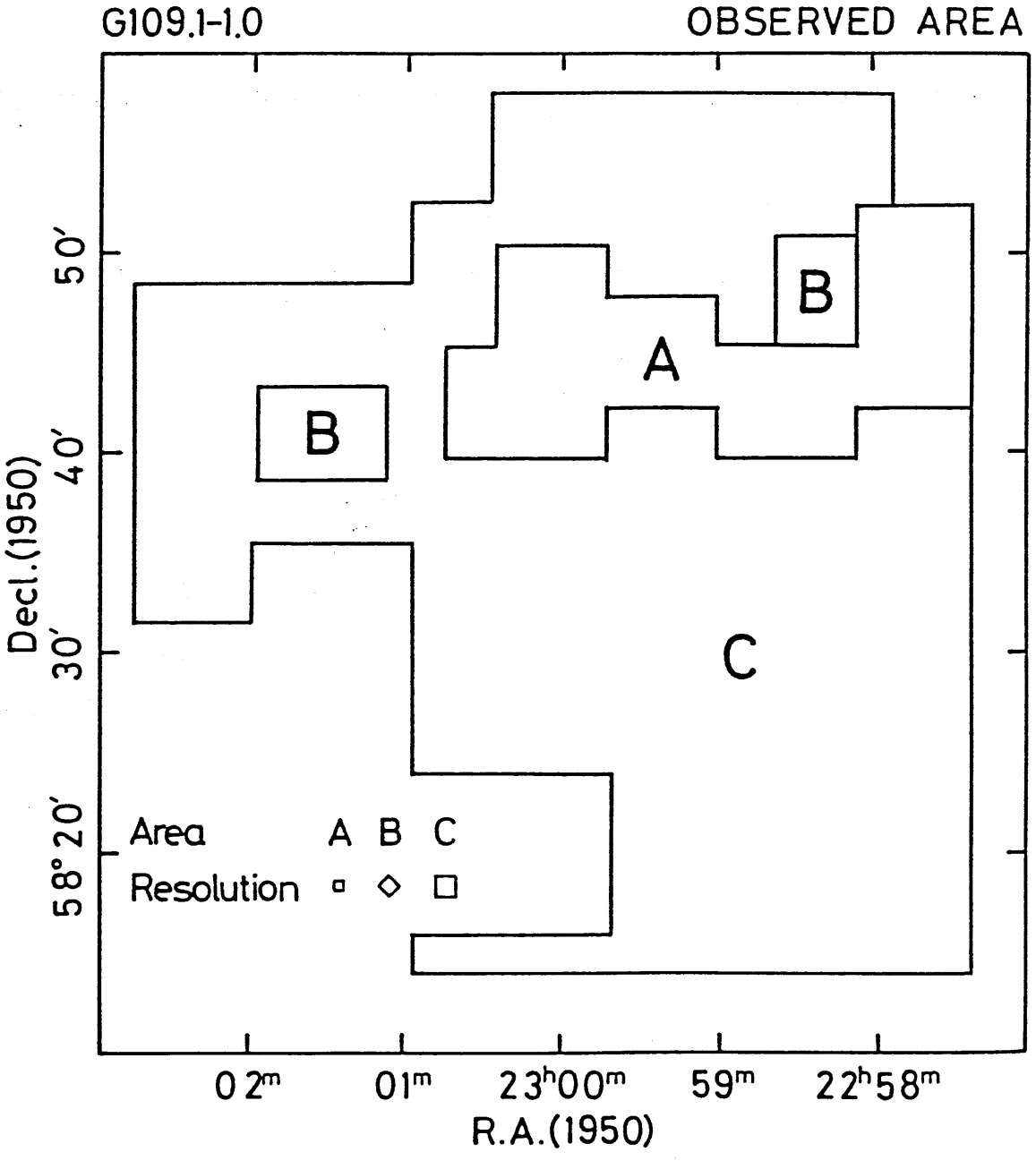
G109.1-1.0
OBSERVED AREA
50′
40′
30′
58°20′
Decl.(1950)
B
A
B
C
Area A B C
Resolution
02m
01m
23h00m
59m
22h58m
R.A.(1950)

Fig. 8.

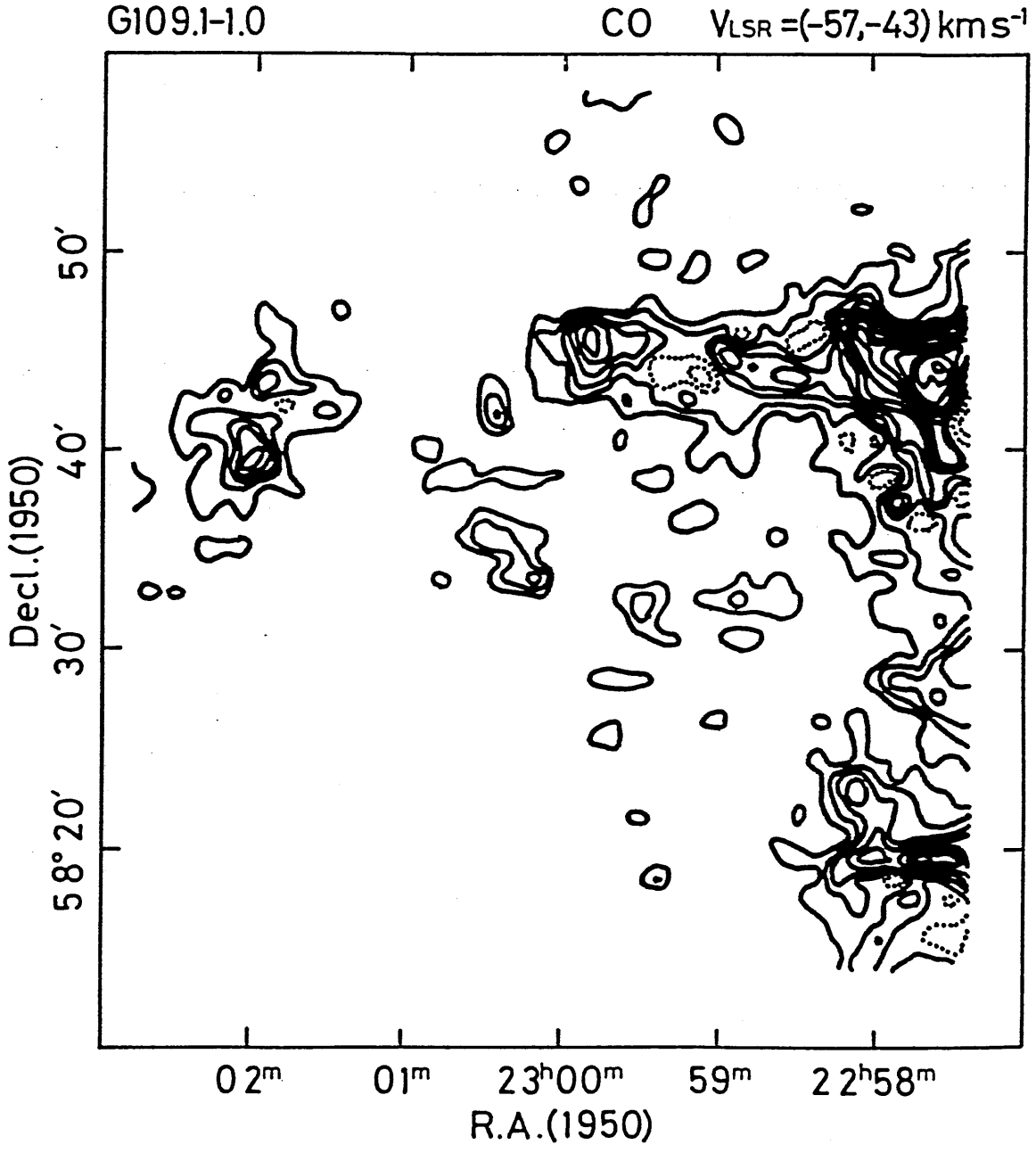
G109.1-1.0
CO
VLSR =(-57,-43) km s-1
50′
40′
30′
58° 20′
Decl.(1950)
02m
01m
23h00m
59m
22h58m
R.A.(1950)

Fig. 9.

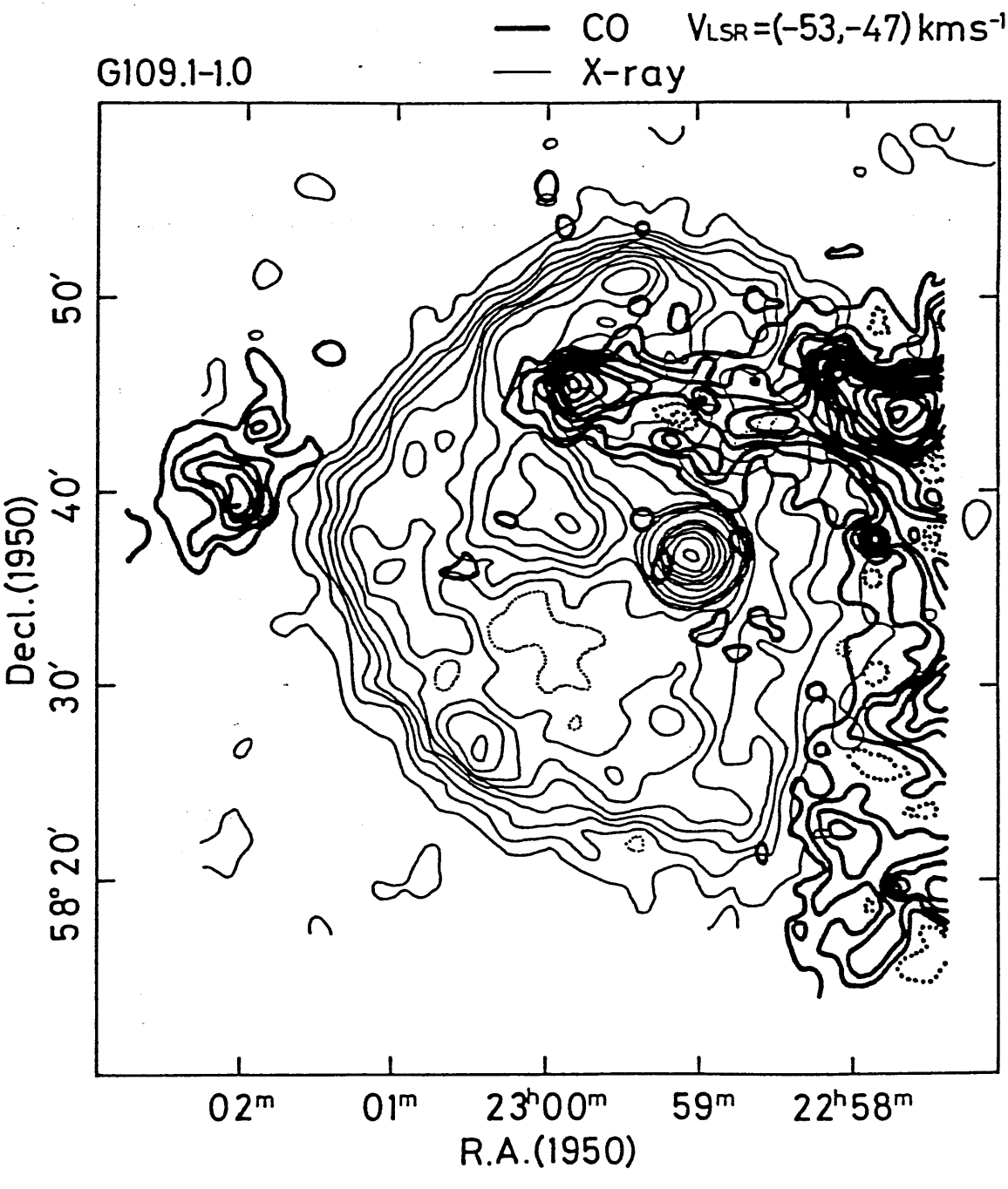
CO VLSR=(-53,-47) kms-1
X-ray
G109.1-1.0
Decl.(1950)
50'
40'
30'
58° 20'
02m
01m
23h00m
59m
22h58m
R.A.(1950)

Fig. 10.

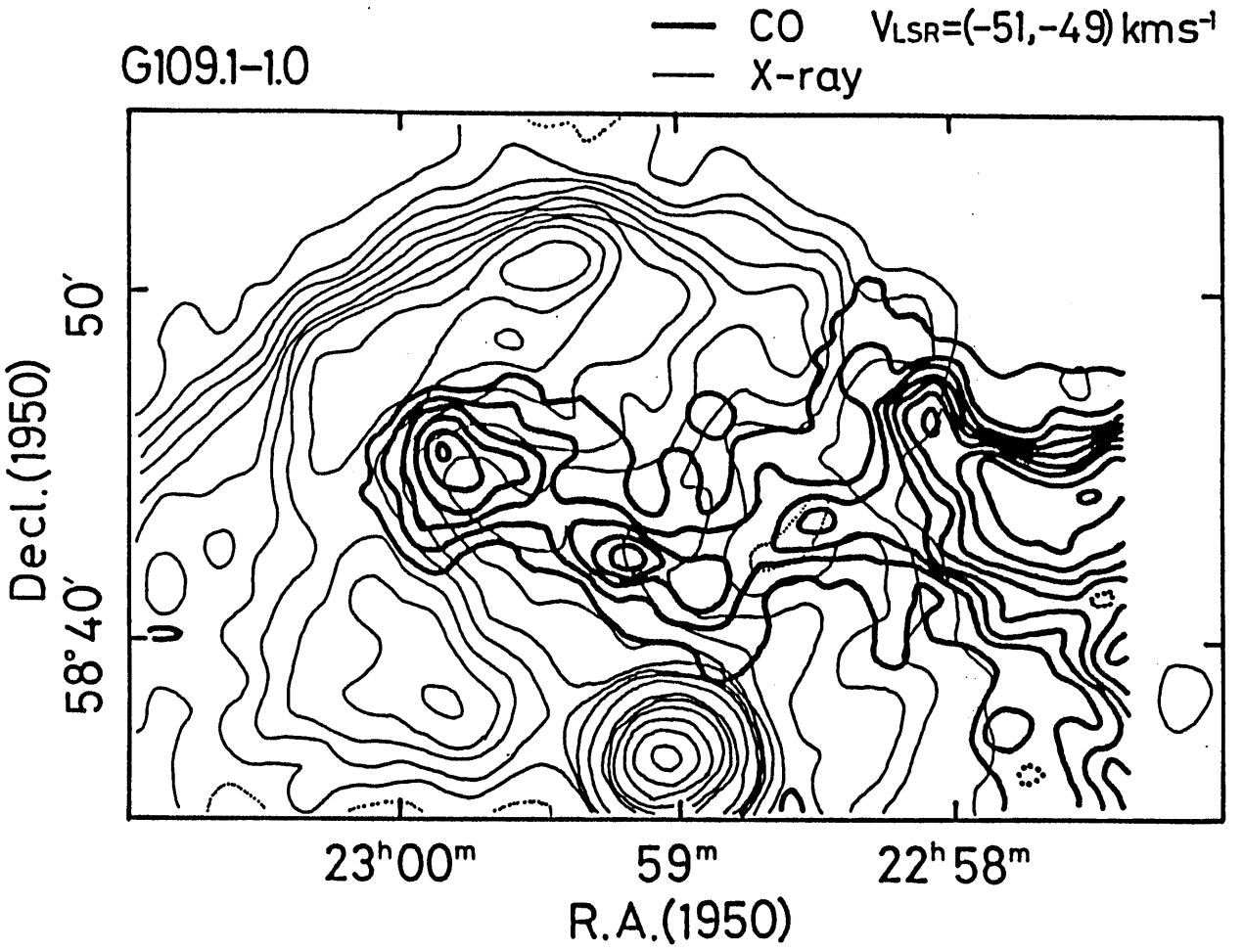
G109.1-1.0
CO VLSR=(-51,-49) kms-1
X-ray
Decl.(1950)
50'
40'
58°
23h00m
59m
22h58m
R.A.(1950)

Fig. 11.

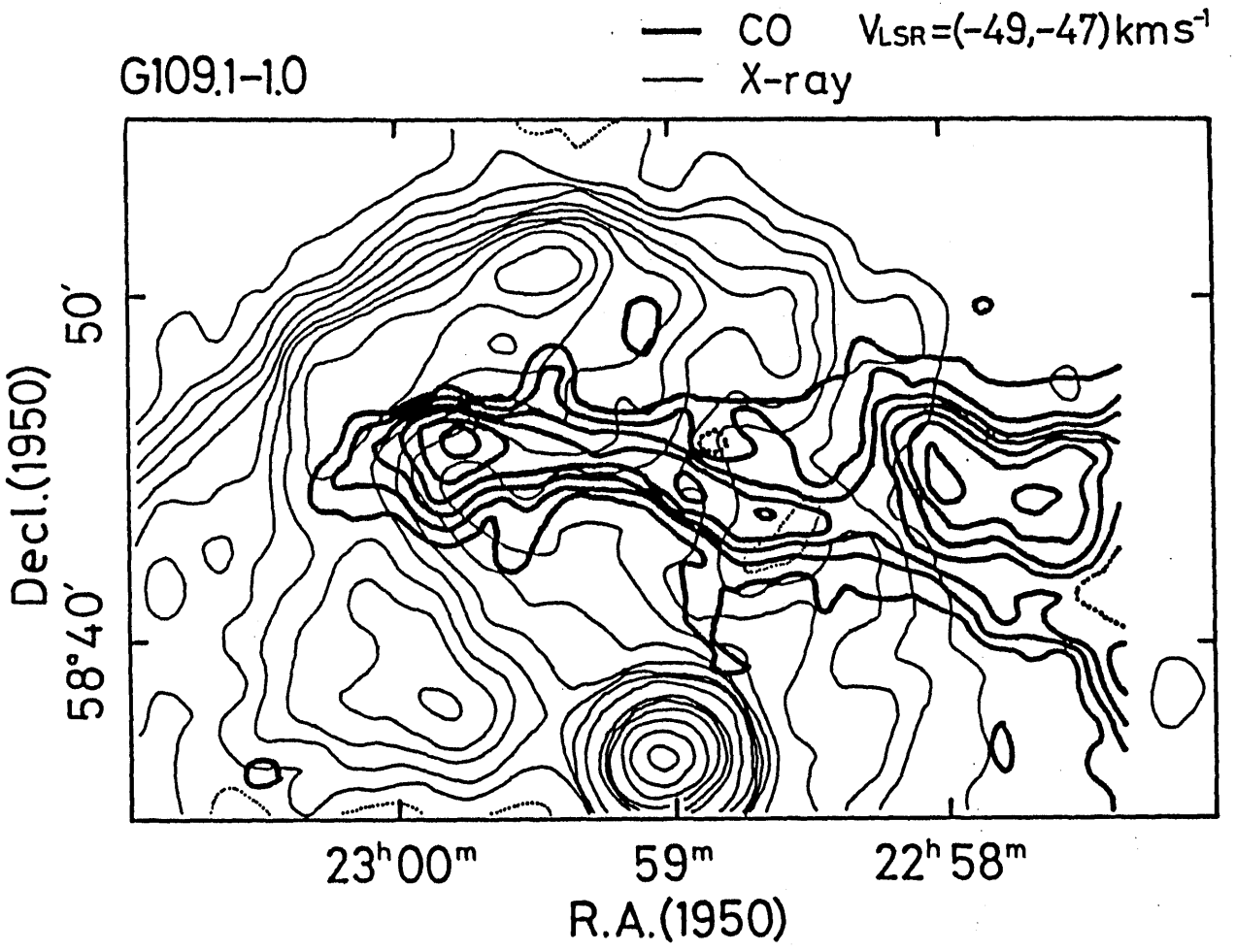
G109.1-1.0
CO VLSR=(-49,-47)kms-1
X-ray
Decl.(1950)
50′
58°40′
23h00m
59m
22h58m
R.A.(1950)

Fig. 12.

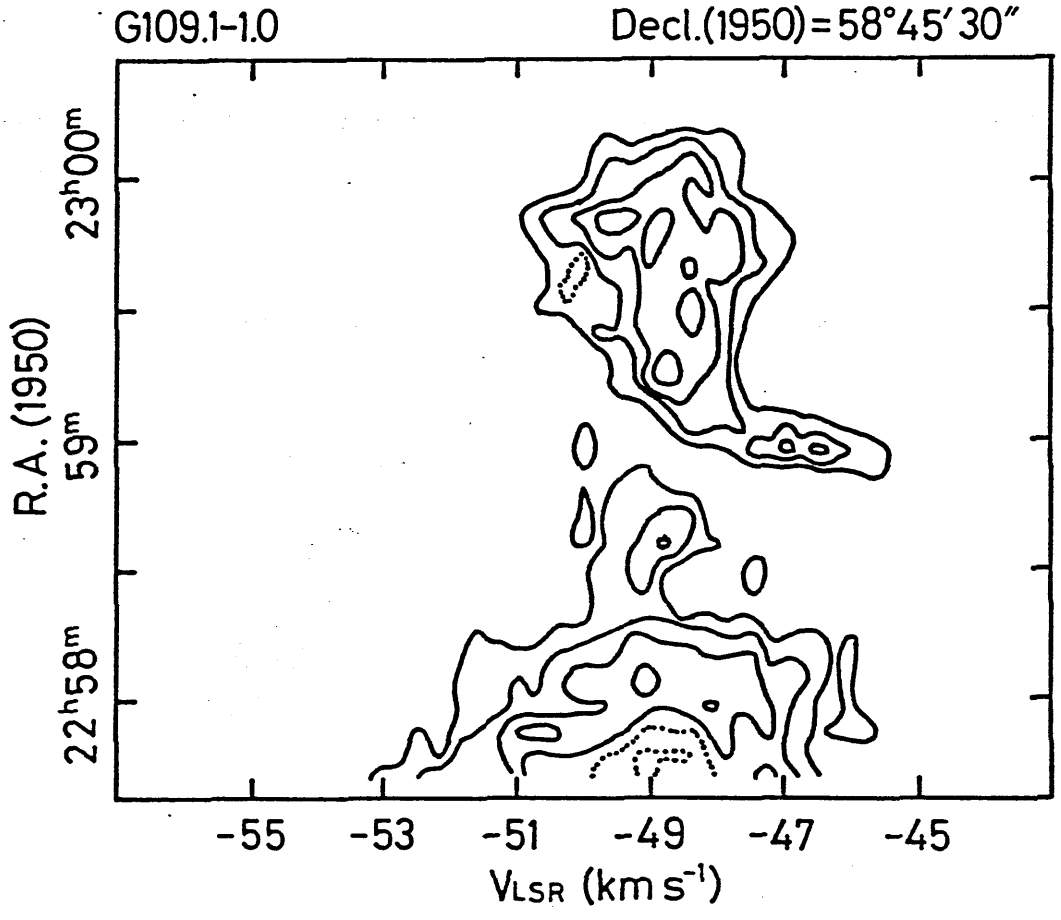
G109.1-1.0
Decl.(1950)=58°45′30″
R.A. (1950)
23h00m
59m
22h58m
-55
-53
-51
-49
-47
-45
VLSR (km s-1)

Fig. 13.

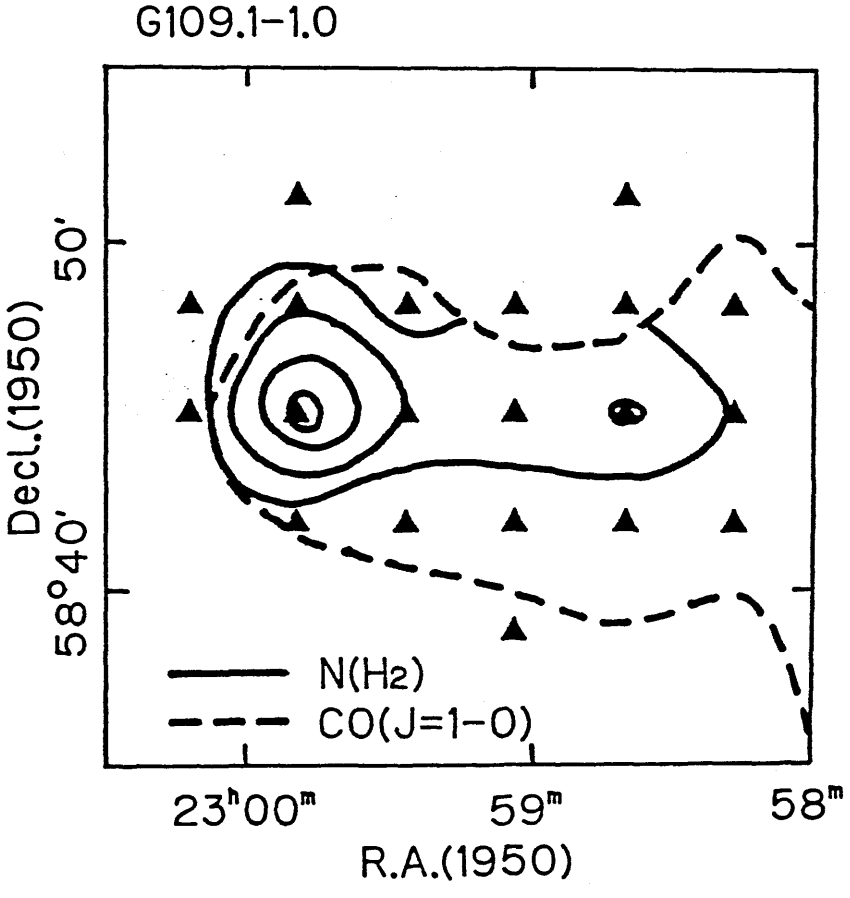

Fig. 14.

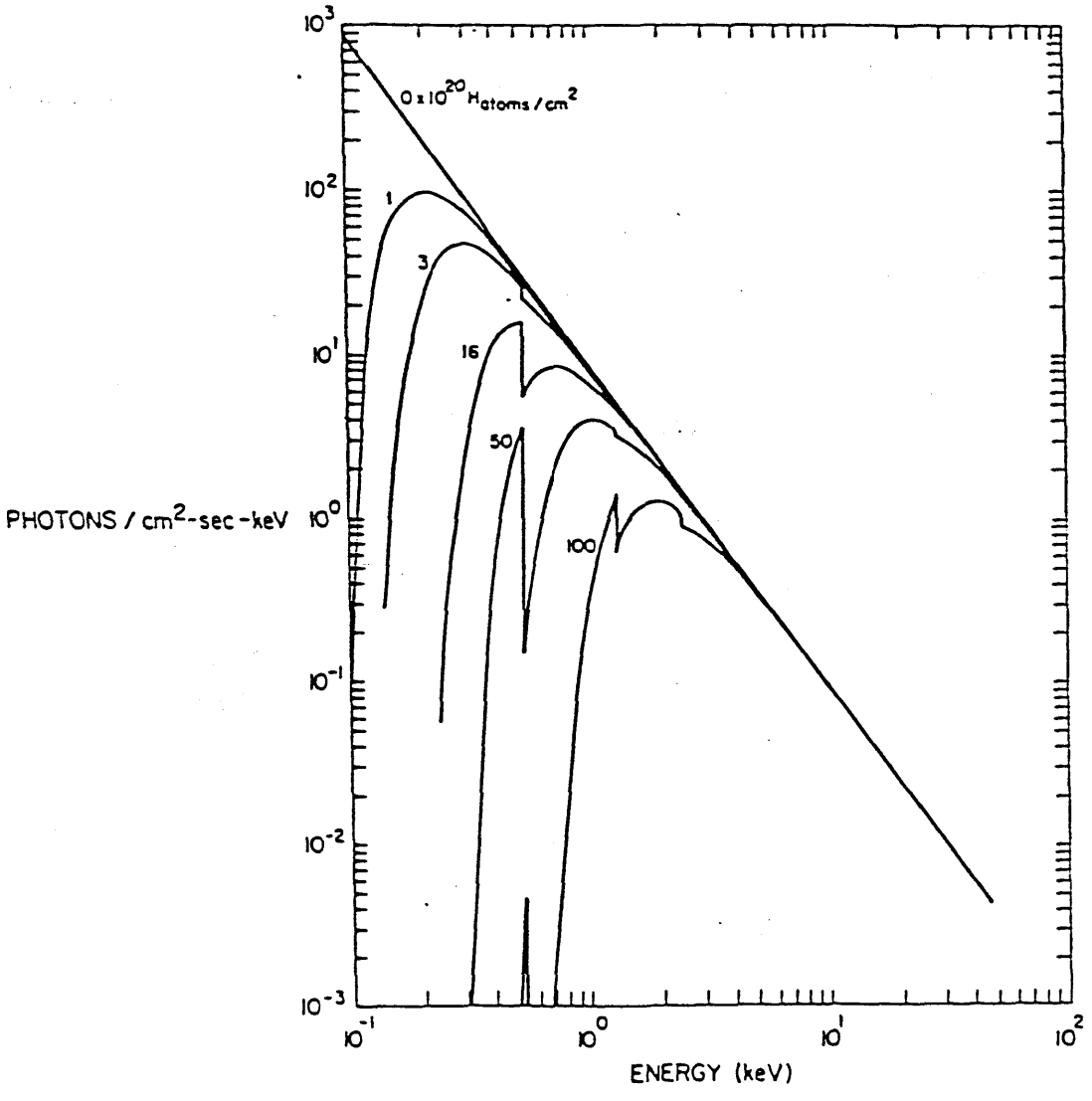
PHOTONS / cm²-sec-keV
ENERGY (keV)
0 x 10²⁰ H atoms / cm²
1
3
16
50
100
10³
10²
10¹
10⁰
10⁻¹
10⁻²
10⁻³
10⁻¹
10⁰
10¹
10²

Fig. 15.

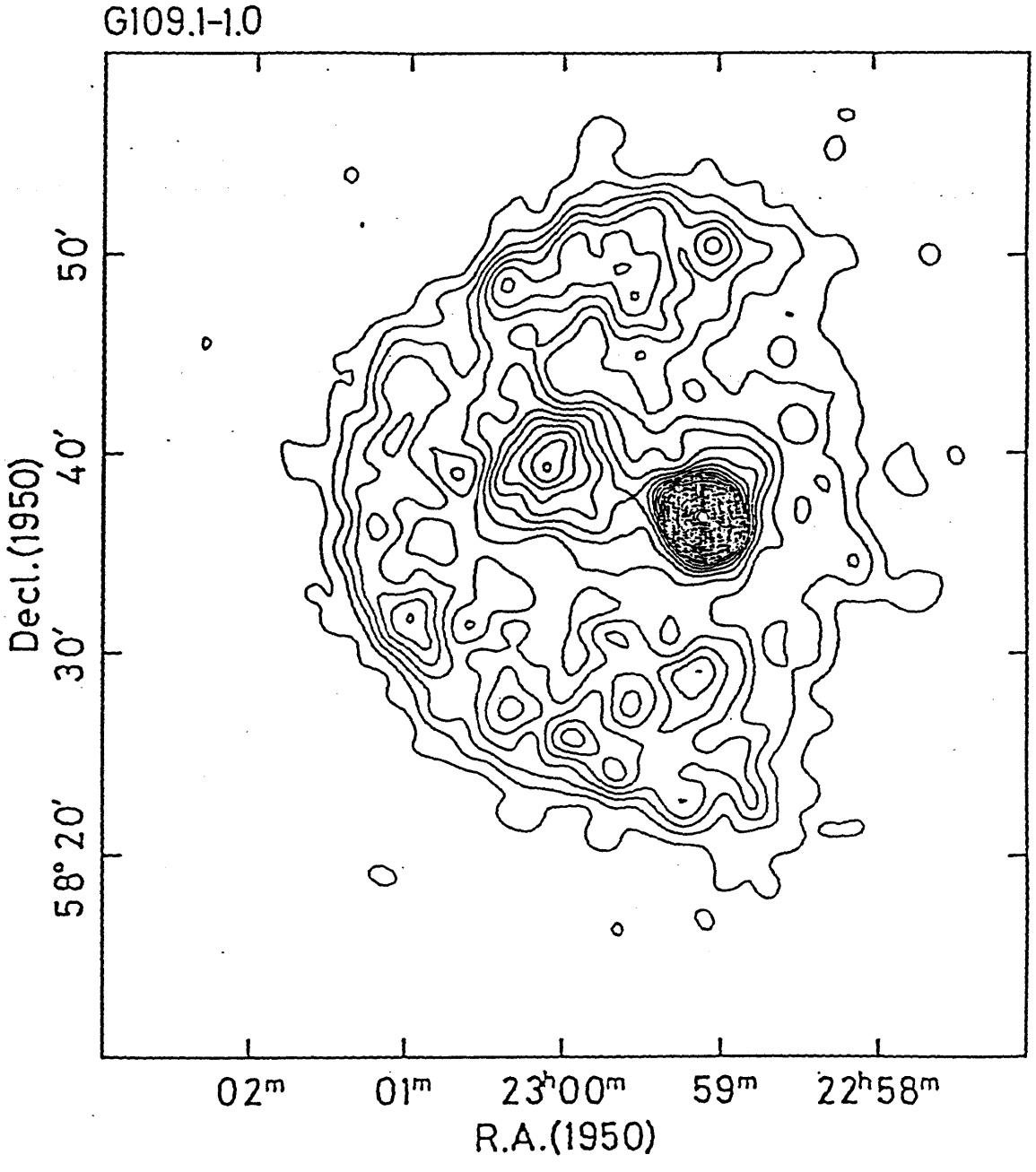
G109.1-1.0
50'
40'
30'
58° 20'
Decl.(1950)
02m
01m
23h00m
59m
22h58m
R.A.(1950)

Fig. 16.

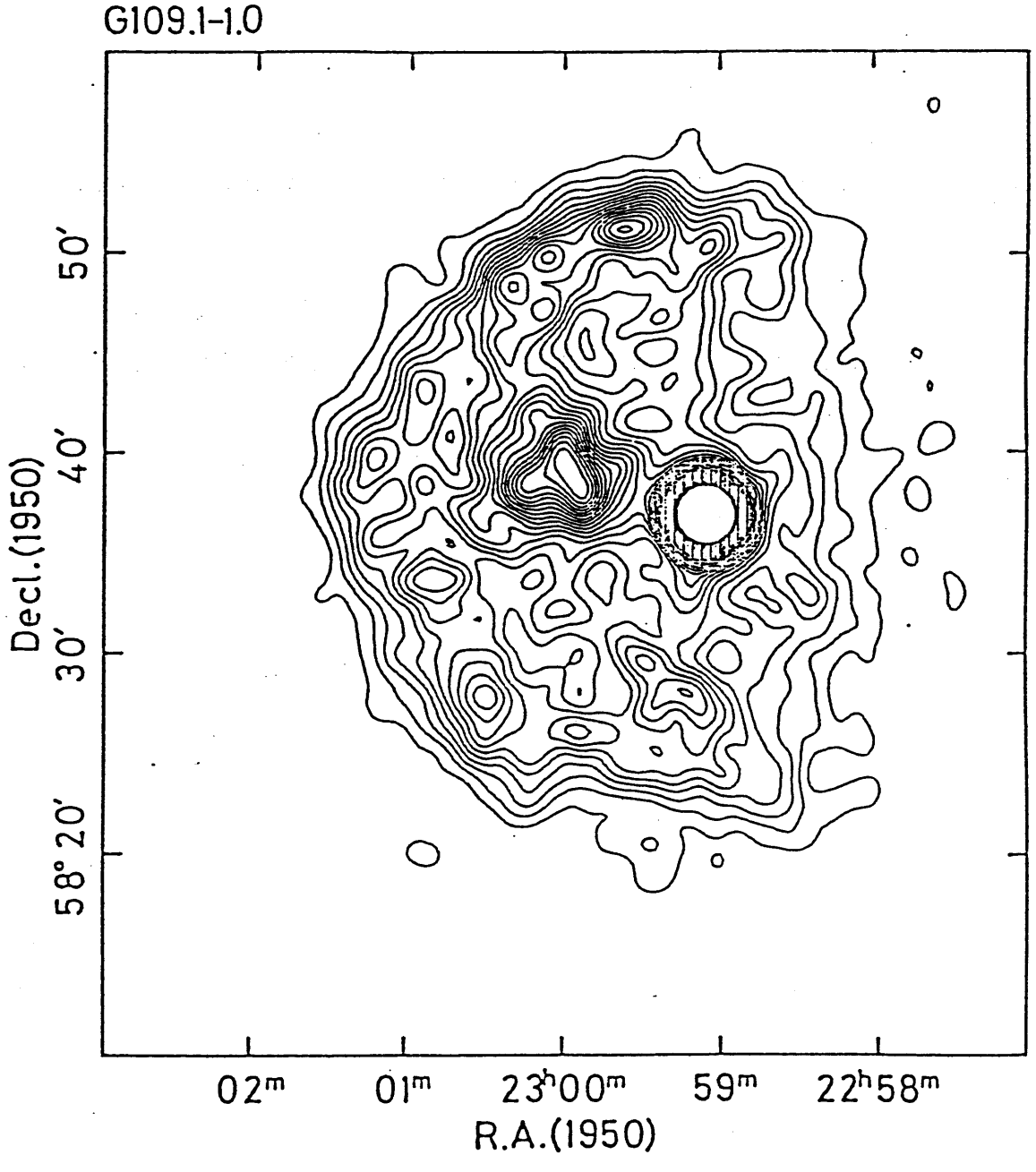
G109.1-1.0
50′
40′
30′
58° 20′
Decl.(1950)
02m
01m
23h00m
59m
22h58m
R.A.(1950)

Fig. 17.

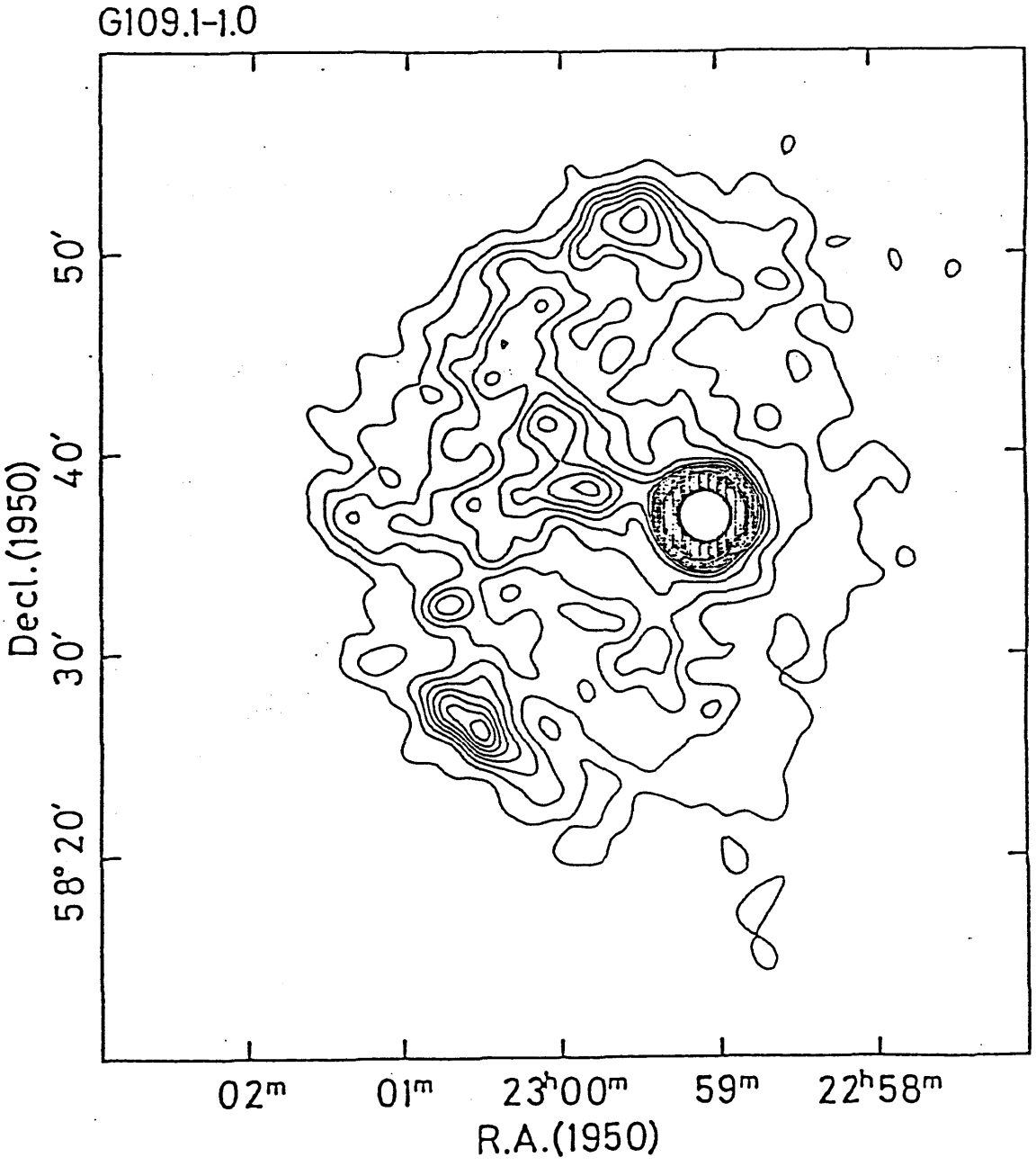
G109.1-1.0
Decl.(1950)
50'
40'
30'
58° 20'
02m
01m
23h00m
59m
22h58m
R.A.(1950)

Fig. 18.

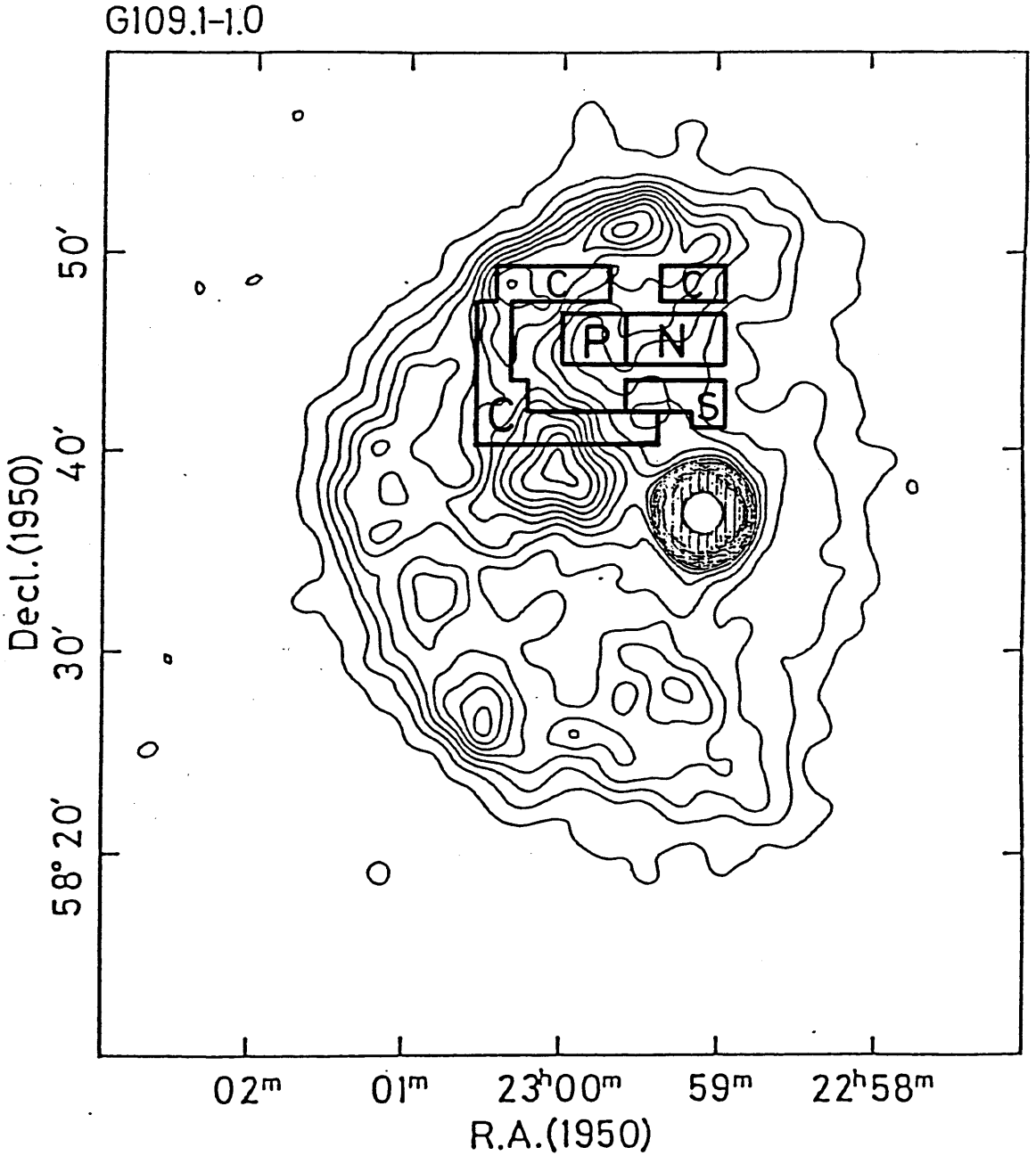
G109.1-1.0
C
C
P
N
C
S
50′
40′
30′
58° 20′
Decl.(1950)
02m
01m
23h00m
59m
22h58m
R.A.(1950)

Fig. 19.

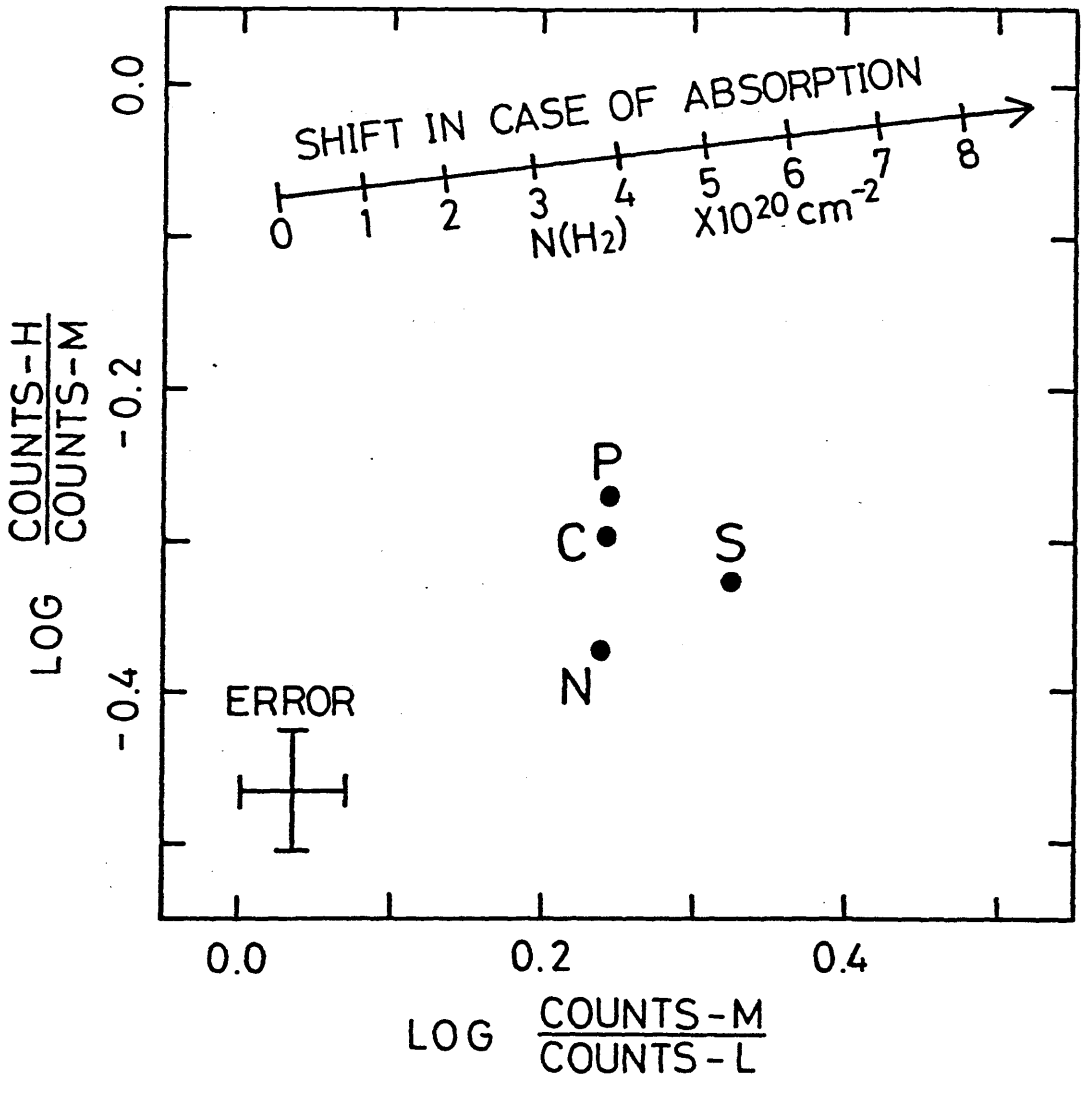
SHIFT IN CASE OF ABSORPTION
0 1 2 3 4 5 6 7 8
N(H2) X10^20 cm^-2
P
C
S
N
ERROR
0.0
-0.2
-0.4
LOG COUNTS-H / COUNTS-M
0.0
0.2
0.4
LOG COUNTS-M / COUNTS-L

Fig. 20.

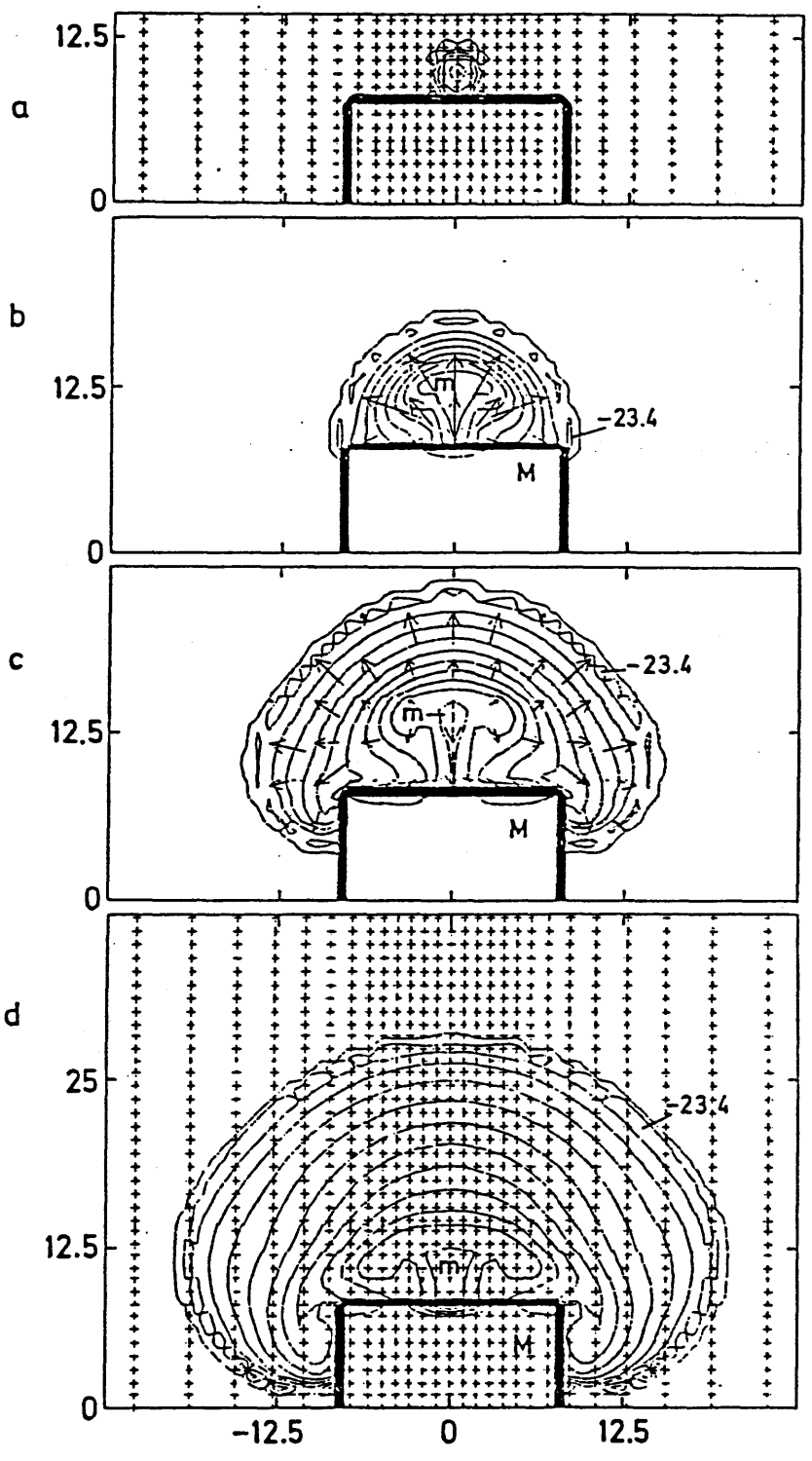

Fig. 21.